SIXTH EUROPEAN ROTORCRAFT AND POWERED LIFT AIRCRAFT FORUM

Paper No. 14

ROTOR BLADE AEROELASTIC STABILITY AND RESPONSE IN FORWARD FLIGHT

P.P. Friedmann and S.B.R. Kottapalli
Mechanics and Structures Department
University of California, Los Angeles
Los Angeles, California, 90024, U.S.A.

September 16-19, 1980

Bristol, England

THE UNIVERSITY, BRISTOL, BS8 1HR, ENGLAND

ROTOR BLADE AEROELASTIC STABILITY AND RESPONSE

IN FORWARD FLIGHT*

P.P. Friedmann and S.B.R. Kottapalli**

Mechanics and Structures Department

University of California at Los Angeles

Los Angeles, California, 90024, U.S.A.

ABSTRACT

The aeroelastic stability and response problem of the coupled flap-lag-torsional dynamics of a hingeless rotor blade in forward flight is treated in a comprehensive manner. The spatial dependence of the partial differential, nonlinear, equations of motion is discretized using a multimodal Galerkin method. The aeroelastic problem is coupled with the trim state of the helicopter obtained from improved, representative, trim procedures. The nonlinear time dependent equilibrium position, or response, about which the equations are linearized is obtained by solving a sequence of linear periodic response problems, using quasilinearization. Numerous results illustrating blade behavior in forward flight are presented.

1. Introduction

In recent years, considerable attention has been focused on a variety of aeroelastic stability and response problems associated with isolated rotor blades and coupled rotor/fuselage systems in hover and in forward flight. A review of this research up to 1976 can be found in Ref. 1. In particular, the hingeless rotor, in which the blades are cantilevered to the hub, has become an increasingly attractive concept due to its mechanical simplicity of construction and favorable control characteristics. A number of successful hingeless rotored helicopters have been built and are in service, both in military and civilian applications, clearly indicating that the hingeless rotor is starting to fulfill its initially envisioned potential.

A further development of the hingeless rotor is the bearingless rotor in which even the pitch change introduced by the pilot through the actuation of the controls is accomplished by introducing a purely elastic twist, thus eliminating the need for the pitch change bearing. Preliminary research and testing of bearingless main rotors and tail rotors indicates even further significant potential for weight saving due to its simple and rugged mechanical configuration. While considerable research on hingeless rotor and bearingless rotor aeroelastic stability problems in hover has been performed[1-6], the studies dealing with the aeroelastic stability and response of such rotors in forward flight, have been much fewer in number and somewhat limited in scope[1,5,7-12].

* This work was supported by the Structures Laboratory AVRADCOM Research and Technology Laboratories and NASA Langley Research Center, Hampton, Virginia under NASA NSG 1578.

** Presently, Dynamics Engineer, Aeromechanics Group, Sikorsky Aircraft, Stratford, Conneticut.

The limited scope of the studies dealing with the forward flight aeroelastic stability and response problems is mainly due to the complicated nature of this subject both from a mathematical modeling point of view (i.e. complicated and lengthy equations) and also because of the need to deal with differential equations with periodic coefficients when solving the stability or response problem, which introduces some mathematical problems inherent in the solution of such equations. This statement can be further clarified by reviewing some of the requirements for reliable modeling of rotary-wing aeroelastic phenomena which are evident from the various references cited in this paper[1-11].

(a) It has been established that for a wide class of aeroelastic stability and response problems, the initial formulation of the equations of motion, in partial differential form, should be nonlinear such that geometric nonlinearities due to the moderate deflections are included in the structural, inertia and aerodynamic operators associated with this aeroelastic problem.

(b) Reliable solutions for stability or response can be obtained by linearizing the nonlinear equations of motion about an appropriate equilibrium position. In aeroelastic problems associated with forward flight the appropriate equilibrium position is a time dependent periodic solution.

(c) Calculation of the time dependent periodic equilibrium position, representing the response solution of the blade is inherently coupled with the trim state of the complete helicopter in forward flight. The degree of sophistication with which this coupling is accomplished can affect the accuracy of the aeroelastic analysis.

The present paper has a number of objectives. First, it extends the formulation presented in Ref. 9, for the coupled flap-lag-torsion dynamics of a hingeless blade in forward flight, which was treated[9] using only one normal mode for each elastic degree of freedom to a complete multimodal representation, in which an arbitrary number of modes can be used to represent the flap, lag and torsional degrees of freedom. This approach retains the realistic aspects of the elastic blade model[9] when compared to the simplified centrally hinged model[7,10-12] and enables one to deal with the response problem, in which a number of modes might be required for meaningful response calculations.

The second objective of the paper is to present improved trim procedures, which are more accurate and comprehensive than previous trim procedures[7,9].

The third objective of the paper is to present a new convenient and efficient method for evaluating the response of periodic systems. The description of a linear version of this method and its application to wind turbine aeroelastic problems was presented in Ref. 13. In the present paper, an extension of the method to nonlinear problems is presented and it is shown that by solving a sequence of linear problems in an iterative manner enables one to obtain solutions for both the nonlinear stability and response problems with a desired degree of accuracy. In mathematical terminology this method is usually denoted by the term quasilinearization. This method is expected to be of considerable practical value in a variety of blade vibration, blade loads and rotor blade aeroelastic stability studies in forward flight.

The results presented illustrate several important aspects of hingeless blade aeroelastic behavior in forward flight. First some typical results from the new trim procedure and its coupling with the aeroelastic analysis are presented. Next it is shown, that various approximations in the periodic equilibrium position can yield quite different stability trends. The importance of the nonlinear terms, in forward flight, on blade response and blade stability is also clarified by the results. Details of the numerical scheme are discussed and the sensitivity of the results to the number of modes used is indicated. Finally, some interesting trends associated with the effect of forward flight on the aeroelastic stability of soft in plane hingeless blades are compared to those of a stiff in plane rotor.

2. Brief Description of the Equations of Motion

The coupled flap-lag-torsional equations of motion upon which this study is based were presented in Ref. 9, a more detailed version of these equations will also be published in the near future[14].

The geometry of the problem is shown in Figs. 1 and 2. The equations of dynamic equilibrium used are based on a considerable number of simplifying assumptions presented in Ref. 9. The most important one, is the assumption that the blade undergoes moderate deflections, implying small strains and finite rotations or slopes. In deriving these equations, it is also assumed that squares of the slopes and products of the slopes are negligible compared to terms of order unity. As a consequence of this assumption, a large number of geometrically nonlinear terms are introduced in the inertia, structural and aerodynamic operators associated with this aeroelastic problem. Some of the higher order nonlinear terms are neglected, in a systematic manner by using an ordering scheme[1,9].

The most important capabilities and limitations of these equations are briefly outlined. The equations are capable of simulating general coupled flap-lag-torsional dynamics of hingeless rotor blades with arbitrary mass and stiffness distributions and offsets between blade elastic axis, cross sectional center of mass and cross sectional aerodynamic center. The aerodynamics are applicable to forward flight at arbitrary advance ratios including an exact representation of reversed flow. Time dependent and radially dependent inflow is also incorporated. Cyclic pitch terms are included. Provisions for including higher harmonic control inputs also exist. Viscous type of structural damping is included in the formulation.

The restrictions present in the equations are due to the neglect of compressibility and dynamic stall effect. Furthermore, quasisteady aerodynamics were used. The equations are restricted to isolated blade dynamics because shaft motions were neglected. It should be noted however, that a version of these equations, including fuselage or shaft motions is also available in the literature[15].

For the sake of completeness, the coupled equations of equilibrium are presented in Appendix B. Two minor terms associated with the structural effects of pretwist are not included in Eq. (B-4), since the proper form of these terms has become available only recently[16,17].

3. Solution of the Equations

3.1 Modal Substitution

The system of general, coupled, partial differential equations of motion presented in Appendix B is transformed into a system of ordinary nonlinear differential equations by using Galerkin's method to eliminate the spatial variable. In this process the elastic degrees of freedom in the problem are represented by the uncoupled free vibration modes of a rotating blade. The elastic degrees of freedom w, v and ϕ are represented by

$$w = \sum_{i=1}^{N_F} \ell g_i(\psi)\eta_i(x_0)$$

$$v = -\sum_{j=1}^{N_L} \ell h_j(\psi)\eta_j(x_0)$$

$$\phi = \sum_{m=1}^{N_T} f_m(\psi)\phi_m(x_0) \tag{1}$$

The various algebraic details as well as the final equations are not presented in this paper and can be found in Reference 14. In the actual implementation of these equations, two elastic modes were used to represent each degree of freedom, i.e. $N_F = N_L = N_T = 2$. After applying Galerkin's method, one obtains a set of coupled nonlinear ordinary differential equations with periodic coefficients. A total of six second order equations are thus obtained.

3.2 Improved Trim Procedures

When solving the nonlinear aeroelastic equations described in the previous section, one must recognize that these solutions are inherently coupled with the trim state of the complete helicopter. The trim state of the helicopter can be obtained by performing a trim analysis. In previous research, relatively simple trim procedures have been used to obtain the trim state[8,9]. In the present study, more comprehensive and improved trim procedures were developed and used. These trim procedures are briefly described below, additional details are available in Reference 14.

These trim procedures have been basically derived for hingeless rotor blades in forward flight and elastic blade flap displacements are included in the analysis. No assumptions are made on the number of harmonics in the flap displacement, this represents considerable improvement on previous studies[8,9], where only first harmonics were included. Variable inflow is included and moment equilibrium is enforced. Azimuthally averaged inertial effects are exactly accounted for. Reversed flow effects are included. Blade precone and elastic center - aerodynamic center offset are also included. A linear built in twist is incorporated in the analysis. Stall and compressibility effects are not considered. Rotor shaft dynamics and tail rotor effects are neglected. The trim equations contain complete provision for higher harmonic pitch control.

Other major assumptions are: (a) The helicopter is in straight and steady flight, (b) Only first mode flapping motion is considered important for trim, higher modes are not included; however, all harmonics associated with the first mode are included, (c) Lead-lag and torsion types of motion are excluded, (d) Nonlinear elastic flap displacement terms are not retained, except in the rotor drag force H where they are important.

The inflow ratio is assumed to be of the form

$$\lambda(\bar{x}_0,\psi) = \lambda_0 k_1(\bar{x}_0) + \lambda_c k_2(\bar{x}_0)\cos\psi + \lambda_s k_3(\bar{x}_0)\sin\psi \tag{2}$$

where λ_0, λ_c and λ_s are specified constants which are determined by the particular inflow model employed. In general

$$\lambda_0 \sim \lambda_0(\alpha_R,\mu,C_T)$$
$$\lambda_c \sim \lambda_c(\alpha_R,\mu,C_T)$$
$$\lambda_s \sim \lambda_s(\alpha_R,\mu,C_T)$$

The total pitch angle θ_G is the sum of the built-in twist, collective and cyclic pitch portions, and any specified pitch due to higher harmonic control $\theta_H(\psi)$, thus

$$\theta_G = \theta_B(\bar{x}) + \theta_0 + \theta_{1c}\cos\psi + \theta_{1s}\sin\psi + \theta_H(\psi) \tag{3}$$

The lift on the blade element is given by[14]

$$\begin{aligned} L = a\rho_A\Omega^2R^3\bar{b}\{ & -\bar{\ell}(\bar{e}_1+\bar{x}_0)\lambda - \mu\lambda\sin\psi - \bar{\ell}\,\beta_p\mu(\bar{e}_1+\bar{x}_0)\cos\psi \\ & - \beta_p\mu^2\sin\psi\cos\psi - \bar{\ell}^2(\bar{e}_1+\bar{x}_0)\overset{*}{\bar{w}} - \bar{\ell}\,\overset{*}{\bar{w}}\sin\psi - \\ & - \ell\mu(\bar{e}_1+\bar{x}_0)\bar{w}_{,x}\cos\psi - \mu^2\bar{w}_{,x}\sin\psi\cos\psi \\ & + \theta_G[\bar{\ell}^2(\bar{e}_1+\bar{x}_0)^2 + 2\bar{\ell}\mu(\bar{e}_1+\bar{x}_0)\sin\psi + \mu^2\sin^2\psi] \\ & + \overset{*}{\theta}_G(\tfrac{3}{2}\bar{b} - \bar{x}_A)[\ell(\bar{e}_1+\bar{x}_0) + \mu\sin\psi]\} \end{aligned} \tag{4}$$

The inflow functions are taken to be

$$k_1(\bar{x}) = 1$$
$$k_2(\bar{x}_0) = k_3(\bar{x}_0) = (e_1 + x_0)/R = \bar{\ell}(\bar{e}_1 + \bar{x}_0)$$

and the constants $\lambda_\theta,\lambda_c,\lambda_s$ are obtained from one of the following inflow models (1) uniform[18] (2) Glauert inflow[18] and (3) Drees type inflow[19].

Integrating the lift expression, the average aerodynamic moment in the thrust direction can be obtained, for one blade, thus

$$T_A = \frac{\ell}{2\pi}\int_0^{2\pi}\int_0^{B} L d\bar{x}_0\, d\psi \tag{5}$$

In the last expression, reversed flow effects are taken into account.

The inplane aerodynamic force H due to one blade is given by[14]

$$H_A = \frac{1}{2\pi}\left[\int_0^{2\pi}\int_0^{B} dH_A d\psi + (F-1)\int_{\pi}^{2\pi}\int_0^{\bar{x}_{RF}} dH_A d\psi\right]$$

where

$$dH_A = \left[-\tilde{p}'_{yA}\sin\psi - (\beta_p + \bar{w}_{,x})L\cos\psi\right]dx_0 \tag{6}$$

$$\tilde{p}'_{yA} = -\rho_A ab\left[-(U'_z)^2 + U'_y U'_z \theta_G - (\tfrac{3}{2}b - x_A)U'_z\theta_G\right] - \rho_A C_{d0} b U'^2_y \tag{7}$$

$$U'_y = -(\Omega R)\left[\mu\sin\psi + \bar{\ell}(\bar{e}_1 + \bar{x}_0)\right] \tag{8}$$

$$U'_z = -(\Omega R)\left[\lambda + \beta_p\mu\cos\psi + \bar{\ell}\,\overset{*}{\bar{w}} + \mu\cos\psi\bar{w}_{,x}\right] \tag{9}$$

It can be also shown[14] that the average inertial contributions for trim, to the pitching and rolling moments are exactly zero. Therefore, only the aerodynamic part is required for trim. The average pitching and rolling moment acting on the blade root, for one blade, are given by

$$M_{pa} = \frac{R^2}{2\pi}\int_0^{2\pi}\left[\int_0^{B} L\,\bar{x}_0 d\bar{x}_0\right]\cos\psi d\psi \tag{10}$$

$$M_{ra} = \frac{R^2}{2\pi}\int_0^{2\pi}\left[\int_0^{B} L\,x_0 dx_0\right]\sin\psi d\psi \tag{11}$$

The last ingredient required in the trim calculation is the steady state flap equation

$$\left[EI\,w_{,xx}\right]_{,xx} - (T\,w_{,x})_{,x} = \tilde{p}_z \tag{12}$$

where

$$T(x) = \Omega^2\int_x^R mx\,dx \tag{13}$$

$$\tilde{p}_z = -ma_z + L \tag{14}$$

$$a_z = \Omega^2[\overset{**}{w} - (\sin\beta_p)^2 w + e_1(\sin\beta_p)^3 + e_1\sin\beta_p(\cos\beta_p)^2$$

$$+ x_0\sin\beta_p\cos\beta_p] \tag{15}$$

only the first elastic flapping displacement is included in the trim procedure thus

$$w = R\eta_1(\bar{x}_0)g_1(\psi) \tag{16}$$

During the actual trim calculations, the steady state flap equation is rewritten in first order state variable form. Subsequently this equation is solved using the method presented in the next section for obtaining the steady state response problem for periodic systems.

The various forces and moments acting on the complete helicopter can be obtained from the ingredients, presented above by multiplying by the number of blades n_b. These forces are schematically shown in Figure 3. In practice, two possible trim calculations are needed:

(a) Propulsive Trim, which simulates actual forward flight conditions. The weight coefficient (approximately equal to the trust coefficient) is given and horizontal and vertical force equilibrium is maintained. In addition, zero pitching and rolling moments are enforced. The complete equations of equilibrium for this case are quite lengthy and are presented in Ref. 14.

When using this trim procedure, μ and C_W are specified and the equations are solved in an iterative manner. The solution yields $g_{1T}(\psi)$, θ_0, θ_{1c}, θ_{1s}, α_R and λ.

(b) Moment Trim or Wind Tunnel Trim, simulates conditions under which a rotor would be usually tested in a wind tunnel. Horizontal and vertical force equilibrium is not required for this case because the helicopter is mounted on a supporting structure as shown in Figure 3. Therefore, only the requirement of zero pitching and rolling moments on the rotor is imposed. The complete trim equations for this case are still quite lengthy and can be found in Ref. 14.

When using this trim procedure, μ, θ_0 and α_R are specified and the equations are solved in an iterative manner. The solution yields C_T, θ_{1s}, θ_{1c}, $g_{1T}(\psi)$ and λ.

Typical trim curves obtained from applying these trim procedures, to a two bladed rotor are shown in Figures 4 and 5. As shown, the main difference between the uniform inflow model and the Glauert model, which uses a linearly distributed inflow with a $\cos\psi$ - component, consists of relatively small differences in the values of θ_{1c} required for trim is the range of $0.20 < \mu < 0.40$.

3.3 Solution of the Blade Equations of Motion

The dynamic equations of equilibrium for the hingeless blade in forward flight are rewritten in first order state variable form. The mathematical form of these equations is given by

$$\{\overset{*}{q}\} = \{Z(\psi)\} + [L(\psi)]\{q\} + \{N(\underset{\sim}{q},\psi)\} = \{F_{NL}(\psi,\underset{\sim}{q},\underset{\sim}{q})\} \tag{17}$$

Since the system is periodic (of period 2π)

$$\{Z(\psi)\} = \{Z(\psi+2\pi)\}$$

and $[L(\psi)] = [L(\psi+2\pi)$

The vector $\{Z(\psi)\}$ represents a known excitation, the matrix $[L(\psi)]$ contains the time dependent coefficients of the linear system, the vector $\{N(q,\psi)\}$ - represents all the nonlinear terms in the equations, and $\{q(\psi)\}$ - is the state of the system. When two flap, two lag and two torsional modes are employed in the analysis, the $\{q(\psi)\}$ column matrix has dimensions of (12x1).

First the linear system is considered

$$\{\overset{*}{q}_L(\psi)\} = \{Z(\psi)\} + [L(\psi)]\{q_L(\psi)\} \tag{18}$$

and the associated homogeneous equation

$$\{\overset{*}{q}_H(\psi)\} = [L(\psi)]\{q_H(\psi)\} \tag{19}$$

Urabe[20] has shown that for characteristic multipliers of the corresponding homogeneous system (19) which are different from one, i.e. a stable homogeneous system according to Floquet theory, one has one and only one periodic solution, of Eq. (18), given by

$$\{q_L(\psi)\} = [\Phi(\psi)]\left\langle\int_0^{\psi}[\Phi(s)]^{-1}\{Z(s)\}ds + ([I] - [\Phi(2\pi)])^{-1}[\Phi(2\pi)]\int_0^{2\pi}[\Phi(s)]^{-1}\{Z(s)\}\,ds\right\rangle \tag{20}$$

The general solution for any inhomogeneous equation, like Eq. (18), whether periodic or not can be mathematically written as[21,22]

$$\{q_L(\psi)\} = [\Phi(\psi)]\{q(0)\} + [\Phi(\psi)]\int_0^{\psi}[\Phi(s)]^{-1}\{Z(s)\}\,ds \tag{21}$$

where in Eqs. (20) and (21) $[\Phi(\psi)]$ is the transition matrix defined by

$$[\Phi(\overset{*}{\psi})] = [L(\psi)][\Phi(\psi)] \tag{22}$$

and $[\Phi(0)] = [I]$

Note that the existence of a unique periodic solution of Eq. (18) is that the determinant of $([I] - [\Phi(2\pi)])$ be nonzero. This is satisfied if all the real parts of the characteristic exponents of the transition matrix, associated with Eq. (19), at the end of one period, $[\Phi(2\pi)]$, $\zeta_i \neq 0$. From Floquet theory if all ζ_i's < 0, the homogeneous system is asymptotically stable; if any one $\zeta_i > 0$, the homogeneous system becomes asymptotically unstable. Some additional comments on this topic can be found in Refs. 14 and 22.

Comparing Eqs. (20) and (21) it is obvious that Eq. (20) corresponds to the general solution of the inhomogeneous system, Eq. (18), with the initial condition given by

$$\{q(0)\} = ([I] - [\Phi(2\pi)]^{-1}[\Phi(2\pi)]\int_0^{2\pi}[\Phi(s)]^{-1}\{Z(s)\}\,ds \tag{23}$$

With this information in mind, the periodic steady state solution of Eq. (18) can be obtained in the following manner:

(a) The initial condition $\{q(0)\}$, Eq. (23) is first evaluated using the transition matrix at the end of a period $[\Phi(2\pi)]$. This matrix is evaluated using the approximate, semianalytical method for determining $[\Phi(2\pi)]$ described in Ref. 23, based upon the fourth order approximation of the matrix exponential. The integral contained in the last term of Eq. (23) is evaluated by taking a constant value of the integrand at each step and performing an ordinary summation. Since normally a revolution, or a period, is divided in over 50 intervals, this is an excellent approximation.

(b) Next, by taking this initial condition, Eq. (23), the linear system, Eq. (18), is integrated numerically using a fourth order Runge-Kutta scheme, with Gill coefficients, which has also been used in Ref. 23. The integration is performed with a constant step size which is also identical to the step size used in evaluating the transition matrix at the end of a period. This means that the use of Eq. (20) is actually, completely bypassed.

(c) Convergence of the method is checked by comparing the displacement quantities obtained for the response with the initial conditions and subsequent revolutions, or periods, i.e. compare $\{q(\psi=0)\}$ with $\{q(\psi=2\pi)\}$, $\{q(\psi=4\pi)\}$ and $\{q(\psi=6\pi)\}$. Normally, excellent converged solutions are obtained within two or three revolutions.

It should be also noted that in Ref. 25, Hsu and Cheng have established a numerical scheme based on direct evaluation of Eq. (20), this method requires considerably more computer time than the method described above.

Next, the solution of the complete nonlinear system, Eq. (17) is considered. The approach used for dealing with this problem is qualilinearization, which is essentially a generalized Newton-Raphson type method possessing second order convergence[25].

Introducing an iteration index k for determining the nonlinear time dependent equilibrium position and performing a first order Taylor series expansion about the $k^{\underline{th}}$ iterate

$$\{\overset{*}{q}\}^{k+1} = \{F_{NL}\}^k + \left[\frac{\partial \underset{\sim}{F}_{NL}}{\partial \underset{\sim}{q}}\right]^k (\{q\}^{k+1} - \{q\}^k) + \left[\frac{\partial \underset{\sim}{F}_{NL}}{\partial \overset{*}{\underset{\sim}{q}}}\right]^k (\{\overset{*}{q}\}^{k+1} - \{\overset{*}{q}\}^k) \tag{24}$$

enables one to write

$$\{\overset{*}{q}\}^{k+1} = [A]^k \{q\}^{k+1} + \{f\}^k \tag{25}$$

Expressing $\{F_{NL}\}$ as

$$\{F_{NL}(\underset{\sim}{q},\overset{*}{\underset{\sim}{q}},\psi)\} = \{Z(\psi)\} + [L(\psi)]\{q\} + \{N_1(\underset{\sim}{q},\psi)\} + \{N_2(\underset{\sim}{q},\overset{*}{\underset{\sim}{q}},\psi)\} \tag{26}$$

substituting Eq. (26) into (24) and carrying out the required algebraic operations, comparing the result with Eq. (25), it can be easily shown that

$$[A]^k = \left([I] - \left[\frac{\partial \underset{\sim}{N}_2}{\partial \overset{*}{\underset{\sim}{q}}}\right]^k\right)^{-1} \left([L(\psi)] + \left[\frac{\partial \underset{\sim}{N}_1}{\partial \underset{\sim}{q}}\right]^k + \left[\frac{\partial \underset{\sim}{N}_2}{\partial \underset{\sim}{q}}\right]^k\right) \tag{27}$$

and

$$\{f\}^k = \left([I] - \left[\frac{\partial \underset{\sim}{N}_2}{\partial \overset{*}{\underset{\sim}{q}}}\right]\right)^{-1} \Big\langle \{Z(\psi)\} + \{N_1(\underset{\sim}{q},\psi)\}^k + \{N_2(\underset{\sim}{q},\overset{*}{\underset{\sim}{q}},\psi)\}^k$$

$$- \left(\left[\frac{\partial \underset{\sim}{N}_1}{\partial \underset{\sim}{q}}\right]^k + \left[\frac{\partial \underset{\sim}{N}_2}{\partial \underset{\sim}{q}}\right]^k\right) \{q\}^k - \left[\frac{\partial \underset{\sim}{N}_2}{\partial \overset{*}{\underset{\sim}{q}}}\right]^k \{\overset{*}{q}\}^k \Big\rangle \tag{28}$$

To initiate the iteration, or solution sequence $\{N_1(q,\psi)\}$ and $\{N_2(q_1,\overset{*}{q},\psi)\}$ are deleted from $\{F_{NL}\}$ and the periodic solution of the linear system, Eq. (18) provides the initial guess thus $\{q\}^o = \{\bar{q}_L\}$ where $\{\bar{q}_L(\psi)\}$ represents the periodic response of Eq. (18) evaluated by the method described at the beginning of this section. The iteration sequence represented by Eq. (25) is applied. Thus, quasilinearization is simply a sequence of linear iterates based on Eqs. (25), (27) and (28). The iterations are terminated when

$$|\{q\}^{k+1} - \{q\}^k| < \varepsilon \tag{29}$$

for all ψ where ε is a prescribed small number. Thus $k = 1$ corresponds to the linearized periodic response and $k = 2$ would correspond to the first approximation of the nonlinear periodic response.

Once the time dependent equilibrium position has been established, the system represented by Eq. (17) is perturbed about this equilibrium position

$$\{q(\psi)\} = \{q(\psi)\} + \{\Delta q(\psi)\} \tag{30}$$

squares of perturbation quantities are neglected, and the stability of the linearized system is determined from Floquet theory, as done previously[8,9], by evaluation the characteristic exponents

$$\lambda_k = \zeta_k + i\omega_k \tag{31}$$

The linearized system is stable when $\zeta_k < 0$

4. Results and Discussion

4.1 Assumptions and Numerical Values Used in the Computations

The equations used in the present study were implemented in a relatively general computer program capable of simulating arbitrary blade configurations. In generating results for this paper, some simplifying assumptions were made in order to reduce the costs of the computations. Furthermore in view of the restricted nature of previous studies, dealing with the forward flight regime, it was felt that the present results are sufficiently general.

The most important simplifying assumptions are listed below:

(a) Mass and stiffness distributions were assumed to be constant along the span of the blade.

(b) Built-in twist θ_B was assumed to be zero.

(c) Cyclic components of the inflow were assumed to be zero, i.e.

$$\lambda_c = \lambda_s = 0$$

$$\lambda_0 = \mu\tan\alpha_R + \frac{C_T}{2\sqrt{\mu^2+\lambda_0^2}} \tag{32}$$

(d) Blade offsets between the blade cross sectional center of mass and elastic axis, and blade cross sectional aerodynamic center and elastic axis were taken to be zero, i.e. $x_I = x_A = x_{II} = 0$

(e) Two rotating mode shapes are used to represent the flap, lag and torsional degrees of freedom respectively. These, first two rotating mode shapes in flap, lag and torsion respectively, are uncoupled mode shapes defined at zero pitch setting. These mode shapes are most convenient for use in an analysis involving forward flight and consequently cyclic pitch variations. Each of these mode shapes are obtained by solving the appropriate free vibration problem by using Galerkin's method based upon five non-rotating modes of a uniform beam in bending and torsion.

The configuration parameters chosen for the cases for which results are presented, were chosen so that the soft in-plane hingeless rotor had properties similar to the Boelkow BO-105 hingeless rotor[26].

The basic parameters, for the case denoted soft-in-plane, were:

$\bar{\omega}_{L1} = 0.732$; $\bar{\omega}_{F1} = 1.125$; $\bar{\omega}_{T1} = 3.176$; $\bar{b} = 0.0275$; $\gamma = 5.5$;

$\sigma = 0.07$; $a = 2\pi$; $C_{d0} = C_{DP} = 0.01$; $n_b = 4$; $B = 1$;

$e_1 = 0$; $R_c = 1$; $\beta_p = 0$; unless otherwise stated

Finally, for all cases except when otherwise stated, on the plots illustrating the various results, the following numerical values were used in the calculations

$$\gamma_F = \eta_{sF1} = \eta_{sF2} = \eta_{sL1} = \eta_{sL2} = \eta_{sT1} = \eta_{sT2} = 0$$

and the various offsets shown in Fig. 3 were also taken to be zero.

4.2 Results

The first set of results presented in Figures 6 through 11 are intended to illustrate typical steady state response plots for the blade tip obtained by applying the effective numerical schemes which were described in Section 3.3. These figures illustrate the response of the soft-in-plane blade, for which the pertinent parameters were presented in the previous section. The helicopter is assumed to be in a state of propulsive trim, with $C_W = 0.005$ and blade response plots for two advance ratios $\mu = 0.20$ and $\mu = 0.40$ are presented.

Figure 6 illustrates the response in the fundamental flap mode $g_1(\psi)$ at $\mu = 0.20$. Two curves are shown, one for $k = 0$ and one for $k = 2$. Recall from the discussion of the quasilinearization technique, presented in Section 3.3, that $k = 0$ corresponds to the linear periodic response in which all nonlinear terms are neglected. Similarly, $k = 1$, corresponds to the linearized response and $k = 2$ corresponds to the first approximation of the fully nonlinear response. There is very little difference, for this case between $k = 1$ and $k = 2$, and therefore, only the results for $k = 2$ were presented. Also, the results for $k = 2$ represent a converged nonlinear period response, i.e, results from the next quasilinearization sequence $k = 3$, are identical to $k = 2$. From a physical point of view this implies, that for this particular case, the effect of the nonlinear terms, on the response, is small, and the response as obtained from linearized equations is accurate.

Similar results for the fundamental lead-lag mode, $h_1(\psi)$, are presented in Fig. 7. Again, the lines for $k = 1$ and $k = 2$ coincide. The effect of the nonlinear terms on the response in this degree of freedom, is much more noticeable, which is consistent with the known sensitivity of lag degree of freedom to higher order nonlinear terms[1]. The results for the fundamental torsional response, $f_1(\psi)$, are presented in Fig. 8, for this case the effect of the nonlinear terms is quite weak. The response for the second flap $g_2(\psi)$, second lag $h_2(\psi)$ and second torsional mode $f_2(\psi)$ are not presented because they are very small.

Figures 9 through 11 illustrate the behavior of the same configuration at a higher advance ratio $\mu = 0.40$. Figure 9 illustrates the flap response. Due to the higher advance ratio, the effect of the nonlinear terms is more noticeable, also noticeable are the higher harmonics when compared to Fig. 6. Also shown in Fig. 9 is the response in the second flap mode $g_2(\psi)$. Two interesting aspects emerge from this figure, since the plots for $k = 0$ and $k = 2$ coincide, it is clear that nonlinear terms have a negligible effect on the response for this case. Furthermore, the second flap response is dominated by the second harmonic. Figure 10 shows the response in the fundamental lag mode $h_1(\psi)$. The importance of the nonlinear terms for this case is quite evident. The fundamental torsional response $f_1(\psi)$ is shown in Fig. 11, and it is relatively insensitive to the effect of the nonlinear terms.

Figures 6 through 11 are representative of the nonlinear periodic equilibrium position $\{q(\psi)\}$ about which the linearized stability boundaries are determined. A considerable amount of numerical experimentation is normally required to determine the optimal stepsize for the periodic response calculations described in Section 3.3. For the cases considered the transition martix, required for the evaluation of Eq. (23) was obtained using 252 steps, and 126 steps were used in the periodic response solution based on the Runge-Kutta scheme. Numerous additional results, on various numerical aspects of these methods can be found in References 14 and 27.

It should be noted that the nonlinear equilibrium position shown in Figs. 6 through 11 is intimately linked to the trim procedures. When performing a trim analysis, the first steady state flapping response, $g_{1T}(\psi)$, is obtained. The trim parameters θ_0, θ_{1C}, θ_{1S}, λ, α_R and C_T are subsequently used to determine the nonlinear periodic equilibrium of the blade. Normally the first flap response $\bar{g}_1(\psi)$ from the aeroelastic response analysis will not be equal to $g_{1T}(\psi)$, i.e. $g_{1T}(\psi) \neq \bar{g}_1(\psi)$. Therefore, for "perfect" matching, iterations have to be performed between the trim program and the aeroelastic response analysis, until some physically meaningful quantities, such as blade hub flapping moments, obtained by these two analyses agree within a desired accuracy. Such iterations can introduce minor changes, in the nonlinear equilibrium potision, however, they were not considered to be cost effective by the authors. For this reason, in generating the results of this paper, this particular iterative feature of the computer program was not exercised.

The effect of forward flight and nonlinearities on the typical soft-in-plane hingeless rotor, for which the parameters were given in Section 4.1, is depicted in Figures 12-14. Figure 12 shows the real part of the characteristic exponent ζ_k for the first lag modes versus advance ratio for propulsive trim. The lines with light circles correspond to results without structural damping while the lines with the dark circles represent, half of a percent of viscous type of structural damping in the fundamental lag mode, Thus $\eta_{SL1} = 0.005$ and $\eta_{SL2} = 0.0008$, the structural damping in the second lag mode is adjusted for the higher frequency of the second lag mode. Since the MBB rotor is a real physical system having structural damping in the vicinity of 1%, at least, it was felt that inclusion of a conservatively small amount of structural damping would yield a more realistic simulation. The real part of the characteristic exponent is an indication of the stability margin of the system, negative values indicate a stable system. The lines with $k = 0$ correspond to neglect of all nonlinear terms. The lines denoted by $k = 1$ correspond to equations linearized about the linear response or equilibrium position, while $k = 2$ corresponds to equations linearized about the converged nonlinear, periodic response obtained from the first quasilinearization step. Thus $k = 3$ would correspond to a second quasilinearization step, which however, is not required because $k = 2$ has converged. It is interesting to note that for this case, the differences between $k = 1$ and $k = 2$ are noticeable only at $\mu = 0.40$. The interesting aspect of these results is the slight degradation in stability, of the first lag mode, between $0.0 < \mu < 0.20$, and the rapid increase in stability with advance ratio thereafter $\mu > 0.20$.

Figure 13 shows the stability of the second lag mode as a function of advance ratio. Again, the dark triangles represent a small amount of structural damping in this mode, $\eta_{SL2} = 0.0008$, while the light triangles correspond to zero structural damping. The interesting aspect here is the low stability margin of this mode in hover and the rapid increase in stability with forward flight.

The characteristic exponents associated with the first two flap modes and the first two torsional modes are presented in Fig. 14. As indicated in the figure, the stability margins in these modes are quite insensitive to forward-flight. Also, it is very interesting to note that only the first flap mode exhibits any sensitivity to the nonlinear terms. The second flap and both the first and second torsional modes are identical for $k = 0, 1, 2$, indicating insensitivity to nonlinear terms.

The conclusion from Figs. 12-14 is that a soft-in-plane hingeless rotor, with properties somewhat similar to the MBB-105 blade, is very stable through the whole flight envelope. These analytical results are also substantiated by the extensive flight test and wind tunnel test results available for this extremely well designed hingeless rotor system[28,29]. It should be noted however, that these trends can be affected by coupling between the rotor and the shaft degrees of freedom which was neglected in the present study[29].

It is interesting to see how this conclusion is modified by changing the fundamental lead-lag frequency from soft-in-plane to stiff-in-plane. Selecting the fundamental in-plane frequency as $\bar{\omega}_{L1} = 1.417$ which can be representative of some stiff-in-plane designs and leaving all other rotor parameters unchanged, as given in Section 4.1, yields the results which are shown in Figs. 15-18. Figure 15 illustrates the real part of the characteristic exponent for the first lag degree of freedom. The plots marked $k = 0$, $k = 1$ and $k = 2$ correspond to linear, linearized about a linear response, and linearized about a nonlinear periodic equilibrium position as obtained by quasilinearization, respectively. Clearly, introduction of the nonlinear terms completely changes the results for this case. There is a strong degradation in stability with advance ratio for this case, and the blade becomes unstable around $\mu = 0.38$. Thus, above $\mu = 0.30$ introduction of moderate deflections, or geometric nonlinearities, is strongly destabilizing. The physical reason for this loss of stability is the change in the various structural coupling terms obtained by going from a soft-in-plane design to a stiff-in-plane design.

Figure 16 shows similar results for the real part of the characteristic exponent associated with the second lag mode. Comparing Figs. 13 and 16 shows that the stability characteristics of the second lag mode for a stiff-in-plane design are markedly different from those of a soft-in-plane blade. The second lag mode in Fig. 16, exhibits deterioration in stability with advance ratio up to $\mu = 0.20$, and only thereafter does it exhibit a mild increase in stability.

The real parts of the characteristic exponents for the first two flap modes are presented in Fig. 17. The interesting property exhibited in these curves is the relatively strong effect of the nonlinearities on the second flap mode as indicated by the differences in the curves denoted by $k = 0, 1, 2$. Comparing Figs. 17 and 14, it is clear that these differences were not evident for the soft-in-plane design.

Figure 18 illustrates the behavior of the real part of the characteristic exponents, for the first two torsional modes as a function of advance ratio μ. The strong effect of the nonlinear terms on the first torsional mode is again evident from the difference between the curves for $k = 0$, 1 and 2, respectively. This is due to the numerous nonlinear bending-torsion structural coupling terms present in the torsional equations. Comparing Figs. 14 and 18, it is again apparent that this behavior was not present in the soft-in-plane design.

In comparing Figs. 15-18, it is evident that the nonlinear terms are destabilizing for the fundamental lag mode and first two flap modes (except at $\mu = 0.40$, for the first flap) while they are stabilizing for the first torsional mode and have little effect on the second torsional mode. Since these nonlinear terms can be both stabilizing and destabilizing, it is clear that nonlinear analyses, based on moderate deflections, are essential in order to predict blade stability in a reliable manner.

As indicated before, blade aeroelastic behavior is strongly dependent on the trim state. Therefore, the blade configurations described by Figs. 12-18 were also investigated by using the moment trim procedure which would be normally used during wind tunnel testing. For the moment trim case $\alpha_R = 0$ and $\theta_0 = 8.2^0$ (0.1432 rad.)

The results for the soft-in-plane blade are shown in Figs. 19 and 20. The real part of the characteristic exponents associated with the first two lead-lag modes are shown in Fig. 19. Comparing Figs. 12 and 19, it is evident that changes of the stability margin as a function of advance ratio are much milder than for the case of propulsive trim. This is mainly due to the different nature of the trim curves for these two procedures which have been illustrated by Figs. 4 and 5. It is also interesting to note that nonlinear terms are stabilizing for the first lag mode and destabilizing for the second lag mode. The mild instability in the second lag mode around $\mu = 0$ will be obviously eliminated by the small amount of structural damping present in all real rotor systems. Figure 20 depicts the real parts of the characteristic exponents for the first two flap and first two torsional modes. As pointed out before, in the discussion of Fig. 14, these modes are completely insensitive to the nonlinear terms, it is only to be expected that by changing the trim procedure, no significant changes are introduced. The reason being, that the trim procedure affects system stability by changing the nonlinear periodic equilibrium position about which the system is linearized.

The behavior of the stiff-in-plane configuration under moment trim conditions is depicted in Figs. 21-23. The real parts of the characteristic exponents for the first two lag modes are shown in Fig. 21. Again the first lag mode is destabilized by forward flight. The second mode, while having lower damping is still relatively insensitive to forward flight. Comparing Figs. 15, 16 and 21, it is evident that similar trends are apparent. However, for the moment trim case, the blade does not experience instability for $0 < \mu < 0.40$, as it did for the propulsive trim case. This means that considerable care has to be exercised in applying stability data from wind tunnel tests to actual flight conditions.

The real parts of the characteristic exponents for the first two flap degrees of freedom are shown in Fig. 22 again the sensitivity of the results to nonlinearities is apparent from the differences between the curves for $k = 0, 1, 2$, respectively. Similar trends are apparent also from the real parts of the characteristic exponents for the first two torsional modes. Comparison of Figs. 17 and 18 with Figs. 22 and 23, show somewhat similar trends.

A number of previous analyses have considered the coupled flap-lag problem in forward flight[1,7,8,12,30]. Therefore, it is interesting to compare the results from the present coupled flap-lag-torsional analysis with a coupled flap-lag analysis in forward flight which is based on identical assumptions[27]. Such a comparison is presented in Figs. 24-26, for the soft-in-plane configuration under propulsive trim conditions with $C_W = 0.005$. The label CFLT on the curves, denotes the results from the coupled flap-lag-torsion analysis. The comparison of real parts of the characteristic exponents for the first lag mode is shown in Fig. 24. It is clear from the figure that the stability margin predicted, for this mode, from the flap-lag analysis is between 250-300% lower than the one predicted by the more accurate coupled flap-lag-torsional analysis. Since the stability margins predicted by the flap-lag analyses are low, these stability margins can easily show exagerated sensitivity to a variety of effects. It should be recognized that this sensitivity can be artificial, because it may be caused by the low damping levels predicted by the flap-lag analysis. Therefore, conclusions drawn from such analyses might be inaccurate when applied to a real rotor.

The real parts of the characteristic exponents associated with the second lag modes, obtained from the coupled flap-lag-torsion analysis (CFLT) and the flap-lag analysis are shown in Fig. 25. In this case, the stability of the second lag mode predicted from the coupled flap-lag analysis is considerably higher than the one predicted from coupled flap-lag-torsion analysis. However, the comment previously made on the reliability of flap-lag analyses continues to apply, because many of these analyses[7,11,12,30] are based on a simple spring restrained model of the blade, in which the second lag mode is nonexistent, or have used only one elastic mode in representing the blade degrees of freedom[8].

The real parts of the characteristic exponents for the first two flap modes, from a coupled flap-lag-torsion analysis (CFLT), are compared to the first two flap modes obtained, from a flap-lag analysis, in Fig. 26. The results show that the damping levels in these modes are predicted quite well by the simplified flap-lag analysis. The damping levels in the flap modes are usually quite high, their insensitivity to modeling errors, implies again that only lowly damped modes, such as the lead-lag mode, can be sensitive to modeling errors.

A considerable amount of additional results were also obtained in the course of this study, however they are not presented here due to lack of space. These results will be available in Ref. 14. Finally, it should be noted that in all response calculations in this study, ten harmonics were retained.

5. Concluding Remarks

In this paper, a relatively comprehensive analysis of the coupled flap-lag-torsional dynamics of a hingeless rotor blade in forward flight was presented. Two elastic modes are used to represent the flap, lag and torsional degrees of freedom, respectively. Furthermore, a convenient numerical method for determining the nonlinear periodic blade response is presented. The aeroelastic analysis has been implemented in a general computer program which could be a very useful analytical tool for both preliminary design work and in correlation studies with wind tunnel or flight test results.

A considerable number of numerical results were presented, from these results the following conclusions can be drawn:

(1) The numerical methods presented provide a very effective means for determining both aeroelastic stability and response. Quasilinearization provides a clear indication of the cases when nonlinear terms due to moderate deflections are important. The results indicate clearly that these terms can be both stabilizing and destabilizing.

(2) Forward flight seems to be stabilizing the blade for a considerable number of cases considered, particularly when the blade is soft-in-plane. Severe degradation in stability with forward flight was observed only for the stiff-in-plane hingeless blade.

(3) The nonlinear time dependent, periodic equilibrium can affect significantly blade stability. Thus, for forward flight, system stability is strongly coupled with the trim state.

(4) Comparisons of coupled flap-lag-torsional analyses with coupled flap-lag analyses indicate that flap-lag analyses can underpredict damping levels in the in plane mode quite severely. Thus conclusions pertaining to blade behavior, based on flap-lag analyses, might be inaccurate and unreliable.

(5) The results indicate that the nonlinearities affect system stability

much more than system response. This implies that for blade vibration and loads calculations approximate analytical models based on linearized or even linear models could be used, provided that blade stability is determined from a more accurate nonlinear analysis such as performed in this study.

(6) Future studies in this field should be aimed at improving the aerodynamics in forward flight, and include compressibility and dynamic stall.

REFERENCES

1. Friedmann, P., "Recent Developments in Rotary-Wing Aeroelasticity", Journal of Aircraft, Vol. 14, No. 11, November 1977, pp. 1027-1041.

2. Hodges, D.H. and Ormiston, R.A., "Stability of Elastic Bending and Torsion of Uniform Cantilever Rotor Blades in Hover with Variable Structural Coupling", NASA TN D-8192, April 1976.

3. Hodges, D.H., "An Aeromechanical Stability Analysis for Bearingless Rotor Helicopters", Journal of the American Helicopter Society, Vol. 24, No. 1, January 1979, pp. 1-9.

4. Staley, J.A., Gabel, R. and MacDonald, H.I., "Full Scale Ground and Air Resonance Testing of the Army-Boeing Vertol Bearingless Main Rotor", AHS Preprint 79-23, presented at the 35th Annual National Forum of the American Helicopter Society, Washington, D.C., May 1979.

5. Bielawa, R.L., Cheney, M.C. and Novak, R.C., "Investigation of a Bearingless Helicopter Rotor Concept Having a Composite Primary Structure", NASA CR-2637, March 1976.

6. Bousman, W.G. and Hodges, D.H., "An Experimental Study of Coupled Rotor-Body Aeromechanical Instability of Hingeless Rotors in Hover", Vertica - The International Journal of Rotorcraft and Powered Lift Aircraft, Vol. 3, No. 3/4, 1979, pp. 221-244.

7. Peters, D.A., "Flap-Lag Stability of Helicopter Rotor Blades in Forward Flight", Journal of the American Helicopter Society, Vol. 20, No. 4, October 1975, pp. 2-13.

8. Friedmann, P. and Shamie, J., "Aeroelastic Stability of Trimmed Helicopter Blades in Forward Flight", Vertica - The International Journal of Rotorcraft and Powered Lift Aircraft, Vol. 1, No. 3, pp. 189-211, 1977.

9. Shamie, J. and Friedmann, P., "Effect of Moderate Deflections on the Aeroelastic Stability of a Rotor Blade in Forward Flight", Paper No. 24, Proceedings Third European Rotorcraft and Powered Lift Aircraft Forum, Aix-en-Provence, France, September 1977.

10. Schrage, D.F. and Peters, D.A., "Effect of Structural Coupling Parameters on the Flap-Lag Forced Response of a Rotor in Forward Flight Using Floquet Theory", Vertica - The International Journal of Rotorcraft and Powered Lift Aircraft, Vol. 3, No. 2, pp. 177-185, 1979.

11. Kaza, K.R.V. and Kvaternik, R.G., Examination of the Flap-Lag Stability of Rigid Articulated Rotor Blades", Journal of Aircraft, Vol. 16, No. 12, December 1979, pp. 876-884.

12. Gaonkar, G.H. and Peters, D.A., "Use of Multiblade Coordinates for Helicopter Flap-Lag Stability with Dynamic Inflow", Journal of Aircraft, Vol. 17, No. 2, February 1980, pp. 112-118.

13. Kottapalli, S.B.R., Friedmann, P.P. and Rosen, A., "Aeroelastic Stability and Response of Horizontal Axis Wind Turbine Blades", AIAA Journal, Vol. 17, No. 12, December 1979, pp. 1381-1389.

14. Friedmann, P.P. and Kottapalli, S.B.R., "Coupled Flap-Lag-Torsional Aeroelastic Stability and Response in Forward Flight", University of California, Los Angeles, School of Engineering and Applied Science Report, to be published in 1980.

15. Warmbrodt, W. and Friedmann, P., "Formulation of Coupled Rotor/Fuselage Equations of Motion", Vertica - The International Journal of Rotorcraft and Powered Lift Aircraft, Vol. 3, No. 3/4, 1979, pp. 245-271.

16. Rosen, A., "The Effect of Initial Twist on the Torsional Rigidity of Beams - Another Point of View", ASME - Journal of Applied Mechanics, Vol. 47, June 1980, pp. 389-392.

17. Hodges, D.H., "Torsion of Pretwisted Beams Due to Axial Loading", ASME - Journal of Applied Mechanics, Vol. 47, June 1980, pp. 393-397.

18. Bramwell, A.R.S., "Helicopter Dynamics", John Wiley and Sons, New York, 1976, pp. 124-125.

19. Drees, M., "A Theory of Airflow Through Rotors and its Application to Some Helicopter Problems", The Journal of the Helicopter Association of Great Britain, Vol. 3, No. 2, July-September, 1949, pp. 79-104.

20. Urabe, M., "Galerkin's Procedure for Nonlinear Periodic Systems", Archives of Rational Mechanics and Analysis, Vol. 20, 1965, pp. 120-152.

21. Wilson, H.K., Ordinary Differential Equations, Addison-Wesley Publishing Co., 1971 (pp. 117).

22. Kottapalli, S.B.R., Friedmann, P.P. and Rosen, A., "Aeroelastic Stability and Response of Horizontal Axis Wind Turbine Blades", AIAA Journal, Vol. 17, No. 2, December 1979, pp. 1381-1389.

23. Friedmann, P., Hammond, C.E. and Woo, T., "Efficient Numerical Treatment of Periodic Systems with Application to Stability Problems", International Journal of Numerical Methods in Engineering, Vol. 11, 1977, pp. 1117-1136.

24. Hsu, C.S. and Cheng, W.H., "Steady-State Response of a Dynamical System Under Combined Parametric and Forcing Excitation", ASME Paper 73-WA/APM 10, 1973, also published in the ASME Journal of Applied Mechanics, 1973.

25. Roberts, S.M and Shipman, J.S., Two Point Boundary Value Problems: Shooting Methods, American Elsevier, New York, 1972, pp. 87-109.

26. Staley, J.A., "Validation of Rotorcraft Flight Simulation Program Through Correlation with Flight Data for Soft-in-Plane Hingeless Rotors", USAAMRDL - TR-75-50, January 1976.

27. Straub, F., "Application of the Finite Element Method to Rotary-Wing Aeroelasticity", Ph.D. Dissertation, University of California, Los Angeles, School of Engineering and Applied Science, April 1980 (to be published as UCLA ENG-report).

28. Huber, H.B., "Effect of Torsion Flap-Lag-Coupling on Hingeless Rotor Stability", AHS Preprint No. 731, 29th Annual National Forum of the American Helicopter Society, Washington, D.C., 1973.

29. Huber, H. and Strehlow, H., "Hingeless Rotor Dynamics in High Speed Flight", Vertica - The International Journal of Rotorcraft and Powered Lift Aircraft, Vol. 1, No. 1, 1976, pp. 39-53.

30. Peters, D.A. and Gaonkar, G.H., "Theoretical Flap-Lag Damping with Various Dynamic Inflow Models", Journal of the American Helicopter Society, Vol. 25, No. 3, July 1980, pp. 29-36.

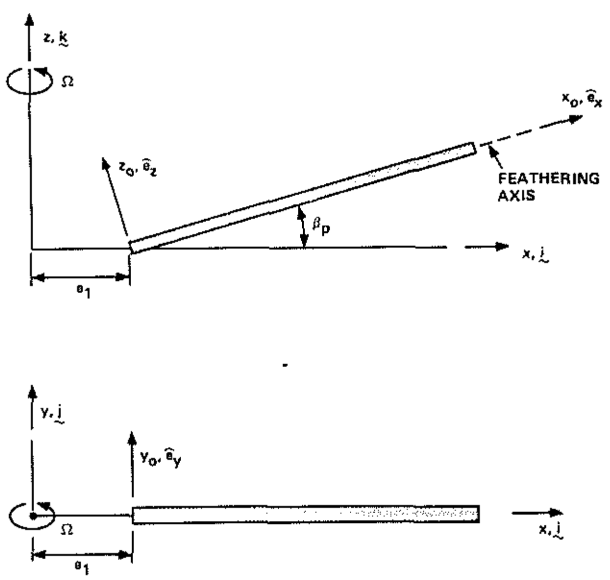

Fig. 1A. Typical Description of the Undeformed Blade in the Rotating System x,y,z $(\underset{\sim}{i},\underset{\sim}{j},\underset{\sim}{k})$

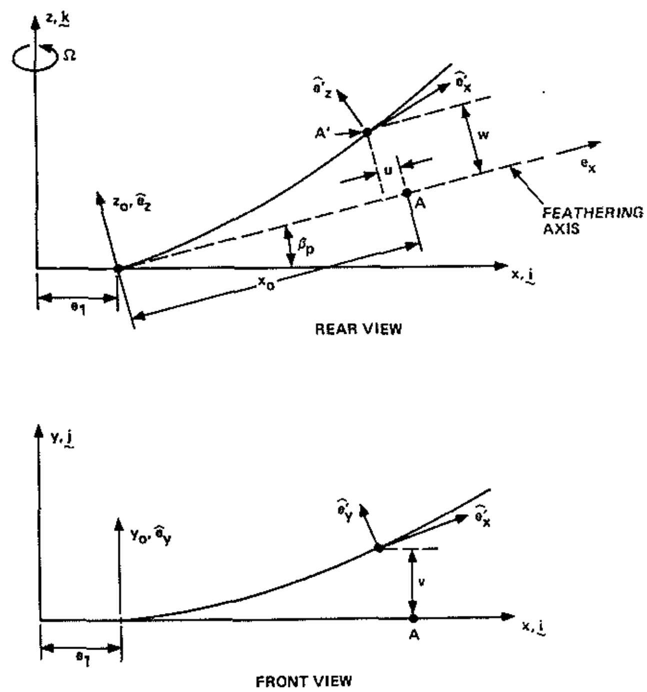

Fig. 1B. Geometry of the Elastic Axis of the Deformed Blade

Appendix A: List of Symbols

$[A(\psi)]^k$	= periodic matrix, Eq. (27)
a	= two-dimensional lift-curve slope
A	= cross sectional area of the blade
a_z	= inertia load used in trim calculation
b	= semi-chord ($\bar{b}$ - nondimensionalized w.r.t ℓ)
B	= tip loss coefficient
$C_W = W/\rho_A \pi (R\Omega R)^2$	= weight coefficient
$C_T = T_A/\rho_A \pi (R\Omega R)^2$	= thrust coefficient
$C_H = H_A/\rho_A \pi (R\Omega R)^2$	= horizontal force coefficient
C_{d0}	= profile drag coefficient
Dp	= parasite drag of helicopter
C_{DP}	= parasite drag coefficient
e_1	= offsets of the blade root from the axis of rotation, shown in Fig. 1
$\hat{e}_x, \hat{e}_y, \hat{e}_z$	= unit vectors in the directions of the coordinates x_0, y_0, z_0, respectively before the deformation
$\hat{e}'_x, \hat{e}'_y, \hat{e}'_z$	= the triad $\hat{e}_x, \hat{e}_y, \hat{e}_z$ after the deformation
E	= Young's Modulus
$f_k(\psi)$	= generalized coordinates for ϕ degree of freedom
f_R, f_{sR}	= offsets shown in Fig. 3
$\{F_{NL}(\psi, \underset{\sim}{q}, \overset{*}{\underset{\sim}{q}})\}$	= complete nonlinear state vector loading, Eq. (17)
$\{f\}^k$	= periodic vector used in quasilinearization, Eq. (28)
$g_{1T}(\psi)$	= fundamental flapping obtained from trim solution of steady state flapping equation, Eq. (12)
$g_i(\psi)$	= generalized coordinates for w degree of freedom
GJ	= torsional stiffness of the blade
g_{SF}, g_{SL}, g_{ST}	= viscous structural damping coefficients in flap, lag and torsion respectively
H_A	= average in plane aerodynamic force, Eq. (6)

$HR, h_s R$ = offsets shown in Fig, 3

$h_j(\psi)$ = generalized coordinates for v degree of freedom

I_2, I_3 = principal moments of inertia of the cross section

$\underset{\sim}{i}, \underset{\sim}{j}, \underset{\sim}{k}$ = unit vectors in the directions x,y and z, respectively

I_b = flapping mass moment of inertia of blade about its root

$I_{m2}, I_{m3} (=k_{m2}^2 m, k_{m3}^2 m)$ = given by $I_{m2} = \int_A \rho\eta^2 dA;\ I_{m3} = \int_A \rho\zeta^2 dA$

i = $\sqrt{-1}$

$[I]$ = unit matrix

$k_1(\bar{x}_0), k_2(\bar{x}_0), k_3(\bar{x}_0)$ = arbitrary functions governing the spatial distribution of the inflow components

$k_{m2}, k_{m3} (\bar{k}_{m2}, \bar{k}_{m3})$ = radii of gyration of cross sectional mass; bars indicate nondimensionalization w.r.t. ℓ

k = iteration index used in quasilinearization

$[L(\psi)]$ = linear coefficient matrix, Eq. (17)

L = unsteady lift, per unit length

ℓ = length of elastic part of the blade

M_{pa} = average pitching moment per blade, Eq. (10)

M_{ra} = average rolling moment per blade, Eq. (11)

$[N(q,\psi)]$ = nonlinear vector, Eq. (17)

$\{N_1(\underset{\sim}{q},\psi)\}, \{N_2(\underset{\sim}{q},\overset{*}{\underset{\sim}{q}},\psi)\}$ = portions of $\{N(\underset{\sim}{q},\overset{*}{q},\psi)\}$, Eq. (26)

n_b = number of blades

$\tilde{p}'_{yA}$ = inplane aerodynamic load used in the trim calculation

$\tilde{p}_z$ = load used in trim calculation, Eq. (13)

$\tilde{p}_x, \tilde{p}_y, \tilde{p}_z$ = components of the distributed external force in directions $\hat{e}_x, \hat{e}_y$ and $\hat{e}_z$, respectively, subscripts I and A denote inertia and aerodynamic contributions respectively

$\tilde{q}_x, \tilde{q}_y, \tilde{q}_z$ = components of the distributed external torque in directions $\hat{e}_x, \hat{e}_y$ and $\hat{e}_z$, subscripts I and A represent inertia and aerodynamic contributions respectively

$\{q\}$ = unknown state vector, Eq. (17)

$\{q_L\}$ = state vector associated with linear, inhomogeneous system, Eq. (18)

$\{q_H\}$ = state vector associated with linear, homogeneous system, Eq. (19)

$\{\bar{q}(\psi)\}$ = nonlinear periodic equilibrium state about which equations are linearized

$\{\Delta q(\psi)\}$ = perturbation of system state, about nonlinear equilibrium position

R = blade radius

R_c = elastic coupling constant

s = dummy variable, Eq. (20)

T = component of the resultant force which acts in the $\hat{e}_x'$ direction (axial tension)

T_A = average thrust used in trim calculations, Eq. (5)

u,v,w = components of the displacement of a point on the elastic axis of the blade in the direction $\hat{e}_x, \hat{e}_y$ and $\hat{e}_z$, respectively

V = velocity of forward flight of helicopter

U_y', U_z' = velocity vector components in the $\hat{e}_y', \hat{e}_z'$ system

x,y,z = rotating coordinate system (Figure 1)

$\bar{x}$ = (x/ℓ)

x_0, y_0, z_0 = initial coordinate system of the blade (Figure 1)

x_A, $(\bar{x}_A = x_A/bR)$ = blade cross-sectional aerodynamic center offset from elastic axis, shown in Figure 2; positive for A.C. before E.A.

x_I = blade cross-sectional mass center of gravity from the elastic axis, shown in Figure 2; positive when in the positive direction of η

x_{II} = offset between the elastic axis and tension center of the cross section of the blade; positive when in the positive direction of η

$\{z(\psi)\}$ = known periodic forcing Eq. (17)

Greek Symbols

α_R = angle of attack of the whole rotor

β_p = preconing, inclination of the feathering axis with respect to the hub plane measured in a vertical plane

γ = $(2\,\rho_A b R^5 a)/I_b$; lock number

γ_F	= flight path angle measured from horizontal
$\gamma_j(x_0)$	= shape functions for v degree of freedom
ζ_k	= real part of the k-th characteristic exponent
$\eta_{SFi}, \eta_{SLi}, \eta_{STi}$	= viscous structural damping coefficients in percent of critical damping, for the flap, lag and torsional modes respectively
η, ζ	= cross-sectional coordinates, see Figure 2
$\eta_i(x_0)$	= shape functions for w degree of freedom
θ_G	= total pitch angle, nonelastic, at pitch bearing about feathering axis
$\theta_B(x)$	= blade pretwist, built-in about elastic axis
θ_0	= collective pitch angle
θ_{1s}, θ_{1c}	= cyclic pitch components
$\theta_H(\psi)$	= higher harmonic pitch
λ_0	= constant part of the inflow ratio
λ_s, λ_c	= cyclic components of the inflow ratio
λ_k	= characteristic exponent associated with the kth degree of freedom
$\mu = V \cos\alpha_R/\Omega R$	= advance ratio
ρ	= density of blade material
ρ_A	= density of air
σ	= blade solidity ratio; blade area/disk area
ϕ	= the rotation of a cross section of the blade around the elastic axis
$\phi_k(x_0)$	= shape functions for ϕ degree of freedom
ψ	= azimuth angle of blade ($\psi=\Omega t$) measured from straight aft position
ω_k	= imaginary part of the kth characteristic exponent
$\bar{\omega}_{F1}, \bar{\omega}_{L1}, \bar{\omega}_{T1}$	= first rotating natural frequencies in flap, lag and torsional respectively, nondimensionalized w.r.t. Ω
Ω	= speed of rotation

Special Symbols

$(\overset{*}{\ })$ = differentiation with respect to ψ

$(\ )_{,x}$ = differentiation with respect to x_0

$(\hat{\ })$ = unit vector

$(\bar{\ })$, $(\underset{\sim}{\ })$ = vector

$\{\ \}$, $(\underset{\sim}{\ })$ = column matrix

$[\ ]$ = square matrix

Additional Symbols

F = reverse flow factor, = −1 for negative lift curve slope in reversed flow region, = 0 for zero lift, =1 for exclusion of all reverse flow effects

x_{RF} = boundary of reversed flow region

$[\Phi(s)]$, $[\Phi(2\pi)]$ = transition matrix for time ψ, and $\psi = 2\pi$ respectively

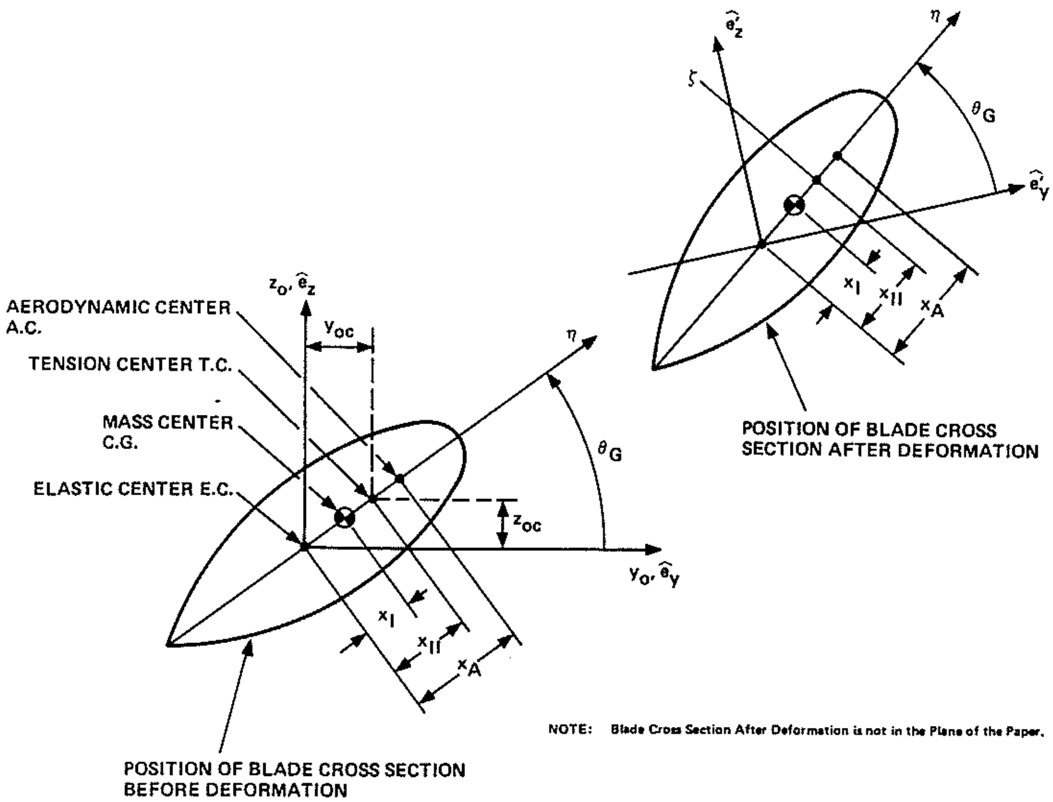

Fig. 2 Blade Cross Section Positions Before and After Deformation

Appendix B: Equations of Motion

The coupled flap-lag-torsional, partial differential, equations of motion for a hingeless blade in forward flight are presented below.

Axial equilibrium

$$T_{,x} + \tilde{p}_{xI} = 0 \qquad \text{(B-1)}$$

Lead-lag equation

$$[E(I_2\cos^2\theta_G + I_3\sin^2\theta_G)v_{,xx} + E(I_2-I_3)\sin\theta_G\cos\theta_G(w_{,xx}-2\phi v_{,xx}) +$$

$$+ E(I_2-I_3)\phi w_{,xx}\cos 2\theta_G]_{,xx} + (GJ\phi_{,x}w_{,xx})_{,x} - (v_{,x}T)_{,x}$$

$$- [m\Omega^2 x_I(x_0 + e_1)\cos\theta_G]_{,x} + m\ddot{v} + 2m\Omega\dot{u} - 2m\Omega\beta_p\dot{w}$$

$$- m\Omega^2 v - m\Omega^2 x_I \cos {}_{G} + g_{SL}\dot{v} - \tilde{p}_{yA} = 0 \qquad \text{(B-2)}$$

Flap equation

$$[E(I_2-I_3)\sin\theta_G\cos\theta_G(v_{,xx} + 2\phi w_{,xx}) + E(I_2-I_3)\phi v_{,xx}\cos 2\theta_G$$

$$+ E(I_2\sin^2\theta_G + I_3\cos^2\theta_G)w_{,xx}]_{,xx} - (GJ\phi_{,x}v_{,xx})_{,x}$$

$$- (w_{,x}T)_{,x} - [mx_I\Omega^2(x_0 + e_1)\sin\theta_G]_{,x} + [2\Omega^2\overset{*}{\theta}_G(I_{m2}\sin^2\theta_G +$$

$$I_{m3}\cos^2\theta_G)]_{,x} + mx_I\Omega^2\overset{**}{\theta}_G\cos\theta_G + m\ddot{w} + 2m\Omega\beta_p\dot{v} +$$

$$+ m\Omega^2\beta_p(x_0 + e_1) + g_{SF}\dot{w} - \tilde{p}_{zA} = 0 \qquad \text{(B-3)}$$

Torsional equation

$$[GJ(\phi_{,x} + v_{,xx}w_{,x})]_{,x} + E(I_2-I_3)[\sin\theta_G\cos\theta_G(v_{,xx}{}^2 - w_{,xx}{}^2)$$

$$- v_{,xx}w_{,xx}\cos 2\theta_G] - g_{ST}\,\Omega\overset{*}{\phi} - \Omega^2\Big\{(I_{m2} + I_{m3})(\overset{**}{\theta}_G + \overset{**}{\phi} + w_{,x}\overset{**}{v}_{,x})$$

$$+ mx_I\cos\theta_G[w_{,x}(x_0 + e_1) - (x_0 + e_1)v_{,x}\phi - \phi\overset{**}{v} + v\phi + \overset{**}{w}$$

$$+ \beta_p(x_0 + e_1) + 2\overset{*}{v}(w_{,x} + \beta_p)] + mx_I\sin\theta_G[- v_{,x}(x_0 + e_1) -$$

$$- \overset{**}{v} + v] + I_{m2}[1 + 2v_{,x})\sin\theta_G\cos\theta_G +$$

$$(- \beta_p v_{,x} + 2\overset{*}{v}_{,x}\phi + \phi)\cos^2\theta_G - (- \beta_p v_{,x} + 2\overset{*}{v}_{,x}\phi + \phi)\sin^2\theta_G$$

$$+ 2\overset{*}{w}_{,x} + 2\overset{*}{v}_{,x}\overset{*}{w}_{,x})\sin^2\theta_G]$$

$$+ I_{m3}[- (1 + 2\overset{*}{v}_{,x})\sin\theta_G\cos\theta_G + (- \beta_p v_{,x} + 2v_{,x}\phi + \phi)\sin^2\theta_G$$

$$- (- \beta_p v_{,x} + 2\overset{*}{v}_{,x}\phi + \phi)\cos^2\theta_G + (2\overset{*}{w}_{,x} + 2\overset{*}{v}_{,x}\overset{*}{w}_{,x})\cos^2\theta_G] \Big\} \qquad \text{(B-4)}$$

Aerodynamic load in the flap equation

$$\tilde{p}_{zA} = a\rho_A bR^3\Omega^2\{(\theta_G + \phi)[2\mu^2 v_{,x}\cos\psi\sin\psi + 2v_{,x}(\bar{x}_0 + \bar{e}_1)(\ell/R)\mu\cos\psi$$

$$+ \mu^2\sin^2\psi + 2\mu\overset{*}{\bar{v}}(\ell/R)\sin\psi + 2\mu(\bar{x}_0 + \bar{e}_1)(\ell/R)\sin\psi$$

$$+ 2\overset{*}{\bar{v}}(\bar{x}_0 + \bar{e}_1)(\ell/R)^2 + (\bar{x}_0 + \bar{e}_1)^2(\ell/R)^2] - \mu^2\cos^2\psi v_{,x}(w_{,x} + \beta_p)$$

$$+ \mu\cos\psi[- v_{,x}\lambda - \overset{*}{\bar{w}}\, v_{,x}(\ell/R) - (w_{,x} + \beta_p)\overset{*}{\bar{v}}(\ell/R) - (w_{,x} + \beta_p)(\bar{x}_o + \bar{e}_1)\ell/R]$$

$$- \mu^2\sin\psi\cos\psi(w_{,x} + \beta_p) + \mu^2\sin^2\psi v_{,x}w_{,x} + \psi\sin\psi[-\lambda-$$

$$- \bar{v}(\ell/R)(w_{,x} + \beta_p) - \overset{*}{\bar{w}}(\ell/R) + 2v_{,x}w_{,x}(\ell/R)(\bar{x}_0 + \bar{e}_1)]$$

$$- \lambda\overset{*}{\bar{v}}(\ell/R) - \overset{*}{\bar{v}}\,\overset{*}{\bar{w}}(\ell/R)^2 - \lambda(\ell/R)(\bar{x}_0 + \bar{e}_1) - \bar{v}(w_{,x} + \beta_p)(\bar{x}_o + \bar{e}_1)(\ell/R)^2$$

$$- \overset{*}{\bar{w}}(\bar{x}_o + \bar{e}_1)(\ell/R)^2 + (\bar{x}_o + e_1)^2(\ell/R)^2 w_{,x}v_{,x} + (1.5 - \bar{x}_A)b(\overset{*}{\theta}_G + \overset{*}{\phi})_G[\psi\sin\psi +$$

$$(\ell/R)(\bar{x}_0 + \bar{e}_1)]\} \qquad \text{(B-5)}$$

Aerodynamic load for inplane equation

$$\tilde{p}_{yA} = - a\rho_A bR^3\Omega^2 \Big\langle (\theta_G + \phi)\{\mu^2\cos^2\psi(v_{,x}w_{,x} + v_{,x}\beta_p)$$

$$+ \mu^2\sin\psi\cos\psi(w_{,x} + \beta_p) + \mu\cos\psi[\lambda v_{,x} + v_{,x}\overset{*}{\bar{w}}(\ell/R) + (\ell/R)\overset{*}{\bar{v}}\, w_{,x} +$$

$$\overset{*}{\bar{v}}\beta_p(\ell/R) + (w_{,x} + \beta_p)(\bar{x}_0 + \bar{e}_1)(\ell/R)] + \mu\sin\psi[\lambda + \bar{v}w_{,x}(\ell/R) +$$

$$+ \bar{v}\beta_p(\ell/R) + \overset{*}{\bar{w}}(\ell/R)] + \lambda(\ell/R)\overset{*}{\bar{v}} + \overset{**}{\bar{v}\bar{w}}(\ell/R)^2 + \lambda(\bar{x}_0 + \bar{e}_1)(\ell/R)$$

$$+ \bar{v}(w_{,x} + \beta_p)(\bar{x}_0 + \bar{e}_1)(\ell/R)^2 + \overset{*}{\bar{w}}(\bar{x}_0 + \bar{e}_1)(\ell/R)^2\}$$

$$- \mu^2\cos^2\psi(w_{,x}^2 + 2w_{,x}\beta_p + \beta_p^2) - \mu\cos\psi[2\lambda\beta_p + 2w_{,x}^2\,\bar{v}(\ell/R)$$

$$+ 4w_{,x}\beta_p\bar{v}(\ell/R) + 2\beta_p^2\bar{v}(\ell/R) + (2w_{,x}\overset{*}{\bar{v}} + 2\beta_p\overset{*}{\bar{w}})(\ell/R)]$$

$$- \lambda^2 - 2\lambda\bar{v}(w_{,x} + \beta_p)(\ell/R) - 2\lambda\overset{*}{\bar{w}}(\ell/R) - 2\overset{*}{\bar{w}}\,\bar{v}w_{,x}(\ell/R)^2 -$$

$$- 2\overset{*}{\bar{w}}\bar{v}\beta_p(\ell/R)^2 - \overset{*}{\bar{w}}{}^2(\ell/R)^2 + [\mu\sin\psi + (\bar{x}_0 + \bar{e}_1)(\ell/R)]w_{,x}v_{,x}[\mu\cos\psi(w_{,x} + \beta_p)$$

$$+ \lambda + \overset{*}{\bar{w}}(\ell/R)] - (1.5 - \bar{x}_A)b(\overset{*}{\theta}_G + \overset{*}{\phi})[-\mu\cos\psi(w_{,x} + \beta_p)$$

$$- \lambda - \overset{*}{\bar{w}}(\ell/R)] + (C_{d0}/a)[2\mu^2 v_{,x}\cos\psi\sin\psi + 2(\ell/R)\mu(\bar{x}_0 + \bar{e}_1)v_{,x}\cos\psi$$

$$+ \mu^2\sin^2\psi + 2(\ell/R)\mu\sin\psi(\overset{*}{\bar{v}} + \bar{x}_0 + \bar{e}_1) + 2(\ell/R)^2\overset{*}{\bar{v}}(\bar{x}_\theta + \bar{e}_1) +$$

$$+ (\ell/R)^2(\bar{x}_0 + \bar{e}_1)^2]\Big\rangle \qquad \text{(B-6)}$$

Aerodynamic torque

$$\tilde{q}_{xA} = \rho_A a(bR)^2R^2\Omega^2 \Big\langle \bar{x}_A\{(\theta_G + \phi)[2\mu^2 v_{,x}\cos\psi\sin\psi +$$

$$+ 2v_{,x}(\bar{x}_o + \bar{e}_1)(\ell/R)\mu\cos\psi + \mu^2\sin^2\psi + 2\mu\overset{*}{\bar{v}}(\ell/R)\sin\psi$$

$$+ 2\mu(\bar{x}_0 + \bar{e}_1)(\ell/R)\sin\psi + 2\overset{*}{\bar{v}}(\bar{x}_o + \bar{e}_1)(\ell/R)^2 + (\bar{x}_\theta + \bar{e}_1)^2(\ell/R)^2]$$

$$- \mu^2\cos^2\psi(v_{,x}w_{,x} + v_{,x}\beta_p) - \mu^2\sin\psi\cos\psi(w_{,x} + \beta_p)$$

$$- \mu\sin\psi[\lambda + w_{,x}\bar{v}(\ell/R) + \beta_p\bar{v}(\ell/R) + \overset{*}{w}(\ell/R)]$$

$$- \mu\cos\psi[w_{,x}\overset{*}{\bar{v}}(\ell/R) + \beta_p\overset{*}{\bar{v}}(\ell/R) + (w_{,x} + \beta_p)(\bar{x}_o + \bar{e}_1)(\ell/R) +$$

$$\lambda v_{,x} + (\ell/R)\overset{*}{\bar{w}}\, v_{,x}] - \lambda\overset{*}{\bar{v}}(\ell/R) - \overset{*}{\bar{v}}\,\overset{*}{\bar{w}}(\ell/R)^2 - \lambda(\bar{x}_o + \bar{e}_1)(\ell/R)$$

$$- v(w_{,x} + \beta_p)(\bar{x}_o + \bar{e}_1)(\ell/R)^2 - \overset{*}{\bar{w}}(\bar{x}_o + \bar{e}_1)(\ell/R)^2 +$$

$$+ w_{,x}v_{,x}[\mu^2\sin^2\psi + 2\mu(\bar{x}_o + \bar{e}_1)(\ell/R)\sin\psi + (\bar{x}_o + \bar{e}_1)^2(\ell/R)^2]\}$$

$$+ (0.5 - \bar{x}_A)(1 - \bar{x}_A)b(\overset{*}{\theta}_G + \overset{*}{\phi})[-\mu\sin\psi - (\ell/R)(\bar{x}_0 + \bar{e}_1)]\Big\rangle \qquad \text{(B-7)}$$

$$\tilde{q}_{yA} = v_{,x}\tilde{q}_{xA} \qquad \text{(B-8)}$$

$$\tilde{q}_{zA} = w_{,x}\tilde{q}_{xA} \qquad \text{(B-9)}$$

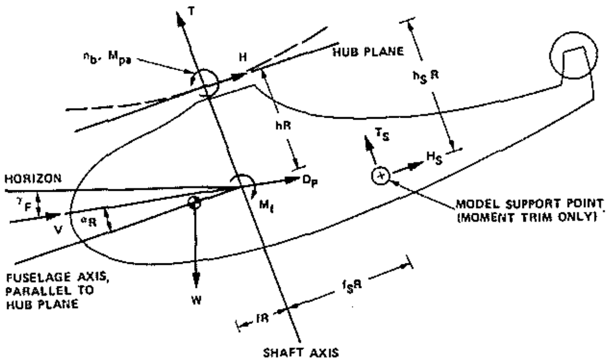

Fig. 3 Longitudinal Forces and Moments for Both Trim Procedures

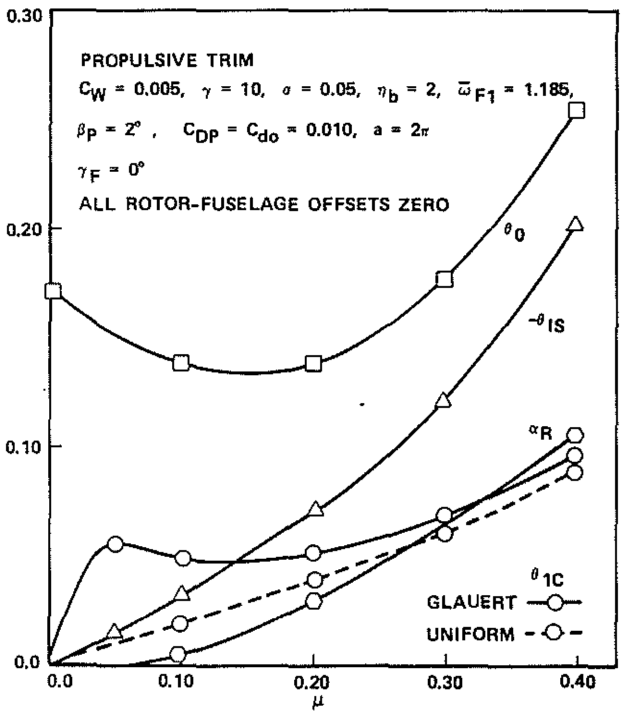

Fig. 4 Typical Propulsive Trim Curves

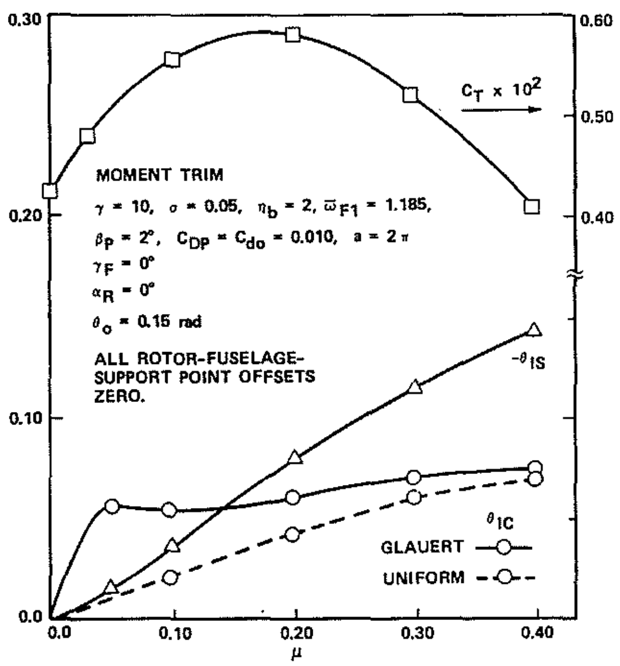

Fig. 5 Typical Moment Trim Curves

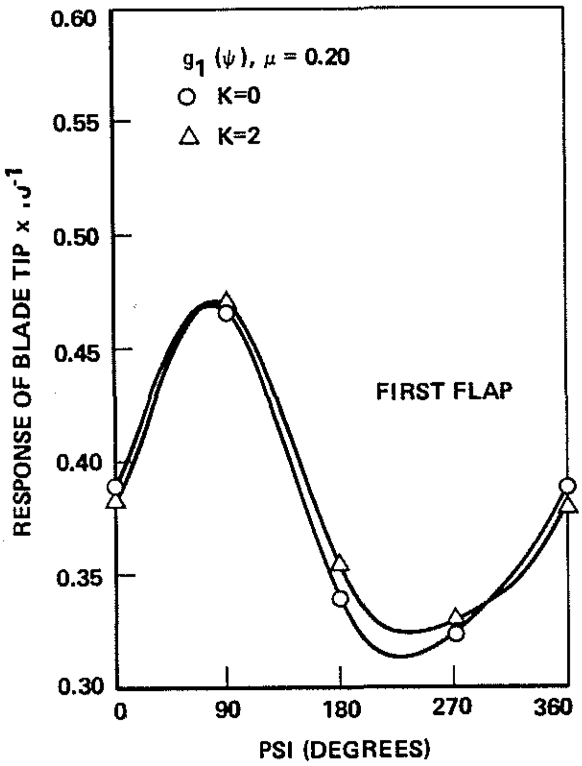

Fig. 6 Soft-in-Plane Configuration Response Propulsive Trim, C_W=0.005

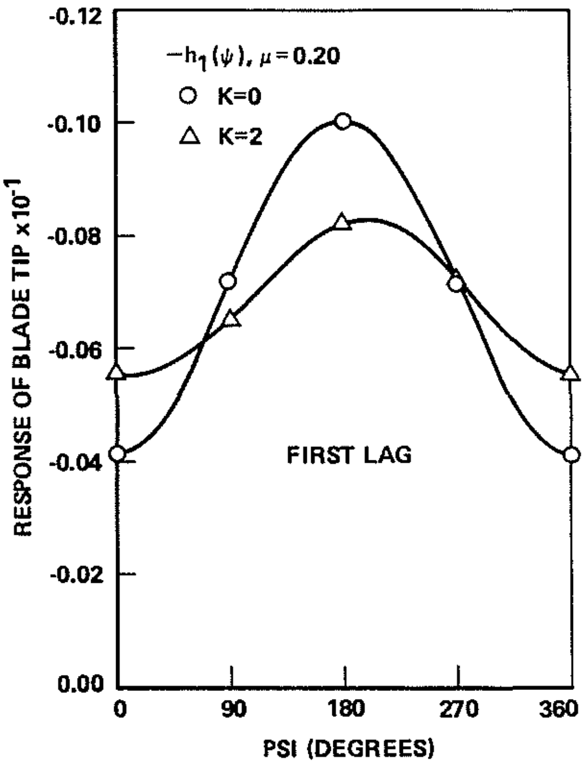

Fig. 7 Soft-in-Plane Configuration Response Propulsive Trim, C_W=0.005

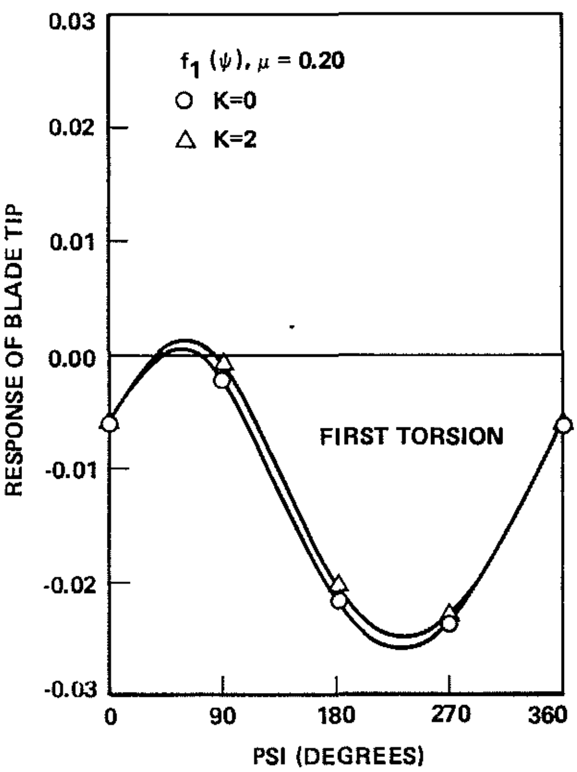

Fig. 8 Soft-in-Plane Configuration Response Propulsive Trim, C_W=0.005

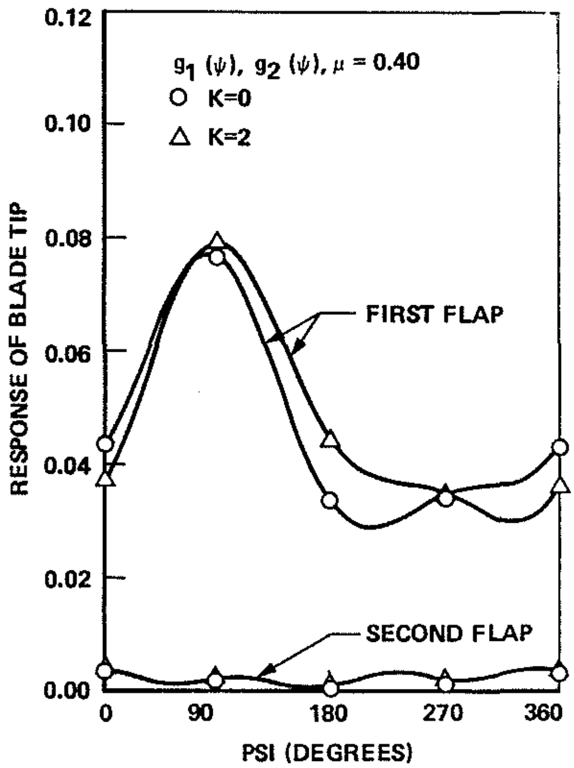

Fig. 9 Soft-in-Plane Configuration Response Propulsive Trim, C_W=0.005

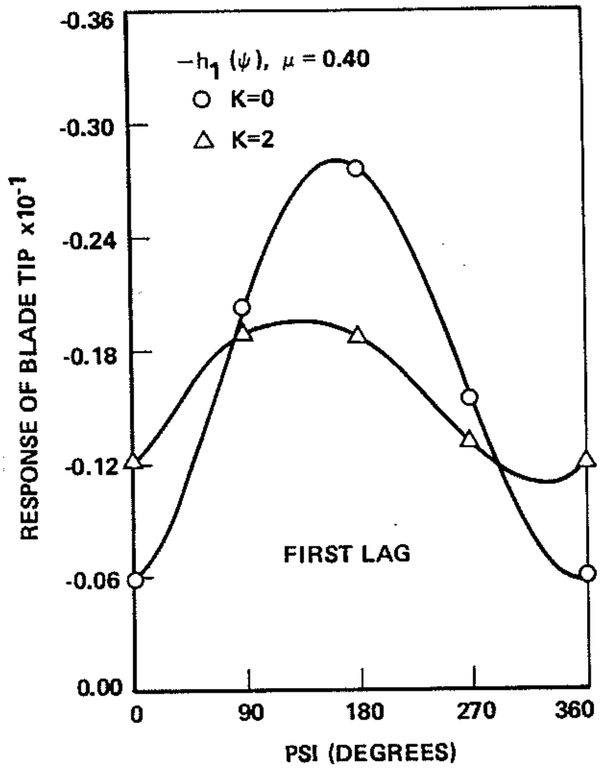

Fig. 10 Soft-in-Plane Configuration Response, C_W=0.005

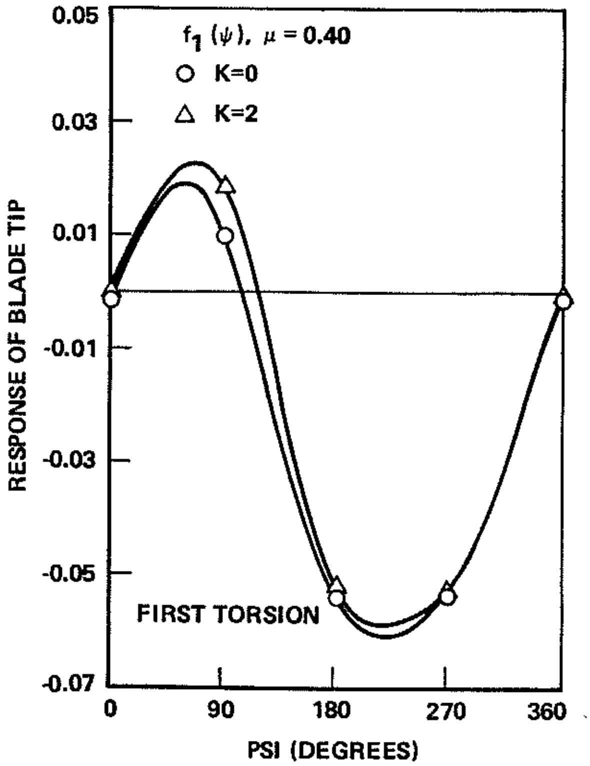

Fig. 11 Soft-in-Plane Configuration Response, C_W=0.005

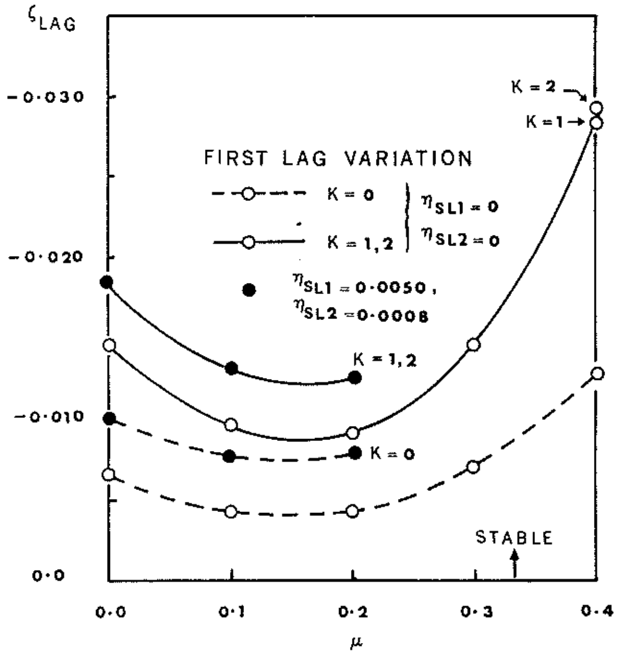

Fig. 12 Soft-in-Plane Configuration Stability, Prop. Trim, C_W=0.005

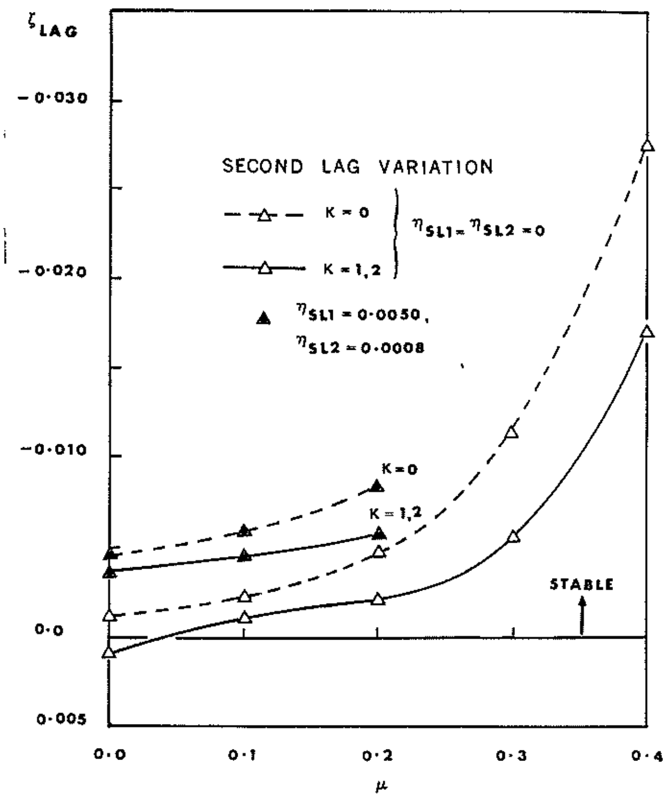

Fig. 13 Soft-in-Plane Configuration Stability, Prop. Trim, C_W=0.005

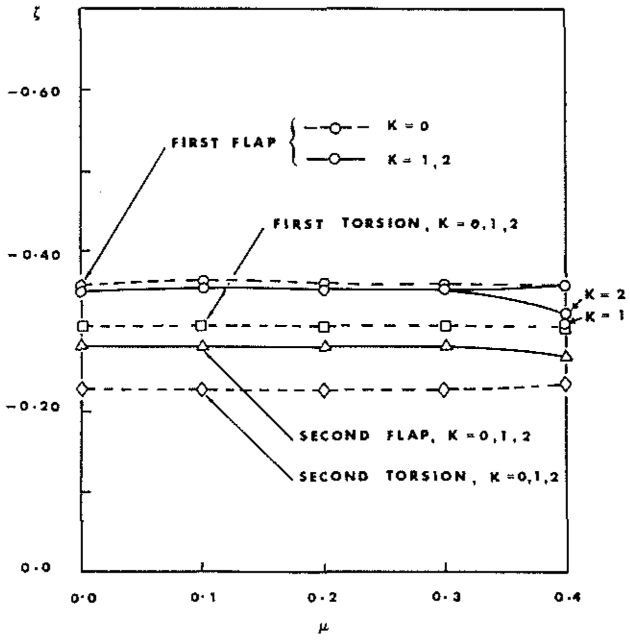

Fig. 14 Soft-in-Plane Configuration Stability, Prop. Trim, C_W=0.005

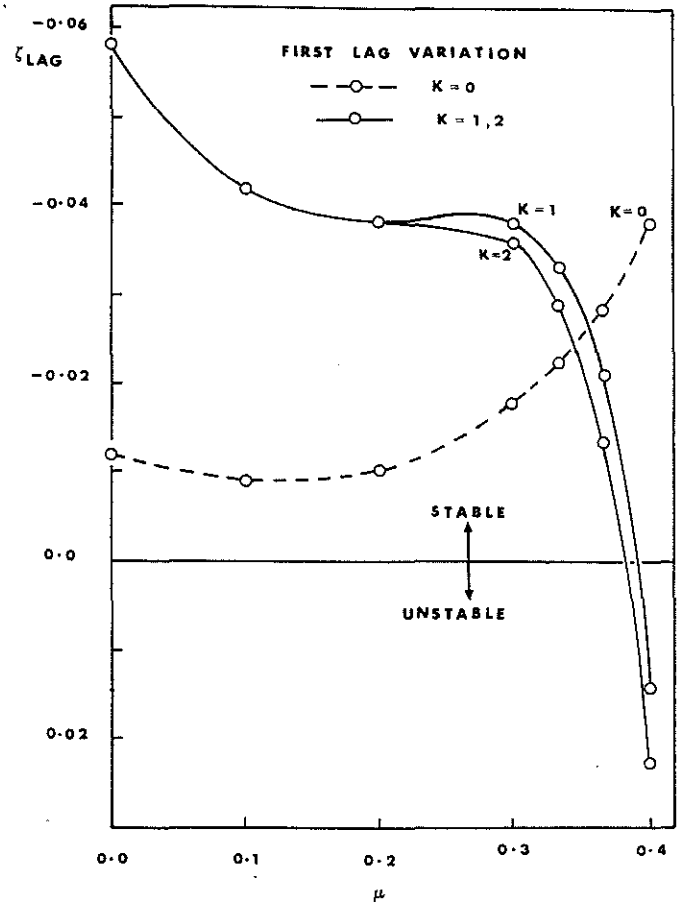

Fig. 15 Stiff-in-Plane Configuration Stability, Prop. Trim, C_W=0.005

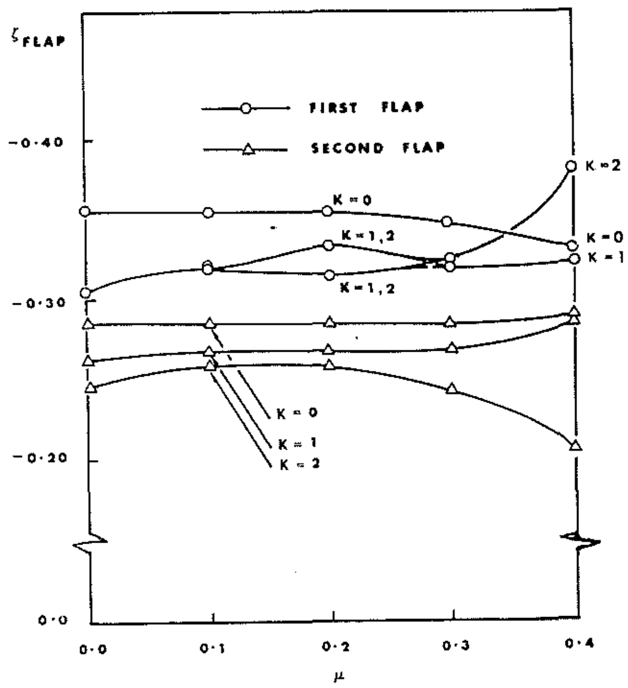

Fig. 17 Stiff-in-Plane Configuration Stability, Prop. Trim, C_W=0.005

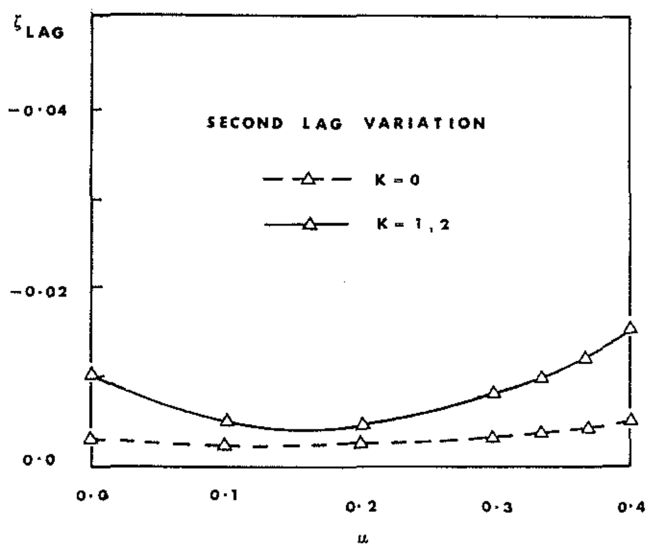

Fig. 16 Stiff-in-Plane Configuration Stability, Prop. Trim, C_W=0.005

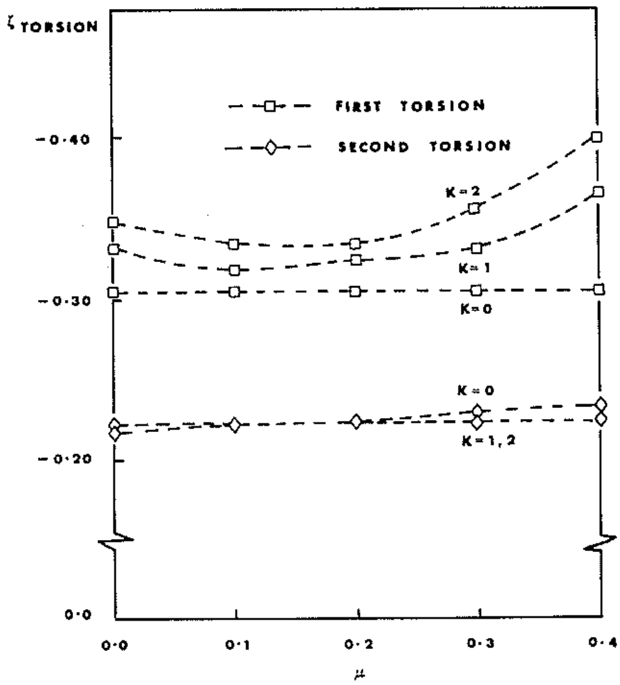

Fig. 18 Blade Stability, Stiff-in-Plane Configuration, Prop. Trim, C_W=0.005

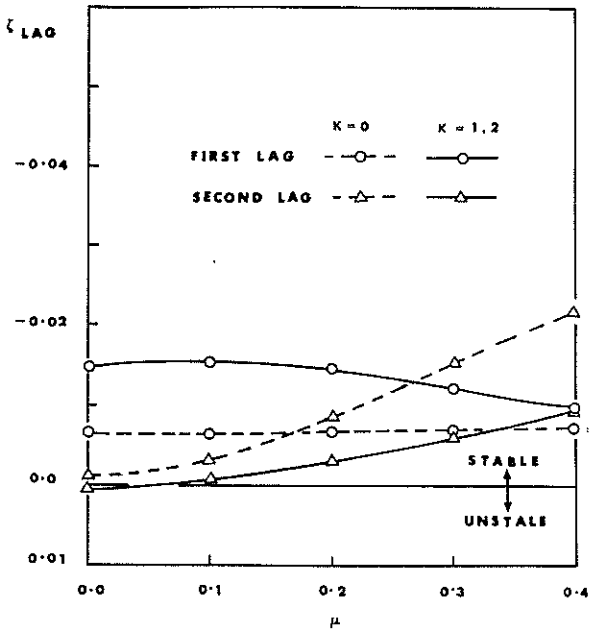

Fig. 19 Blade Stability, Soft-in-Plane Configuration, Moment Trim, θ_0=8.2°

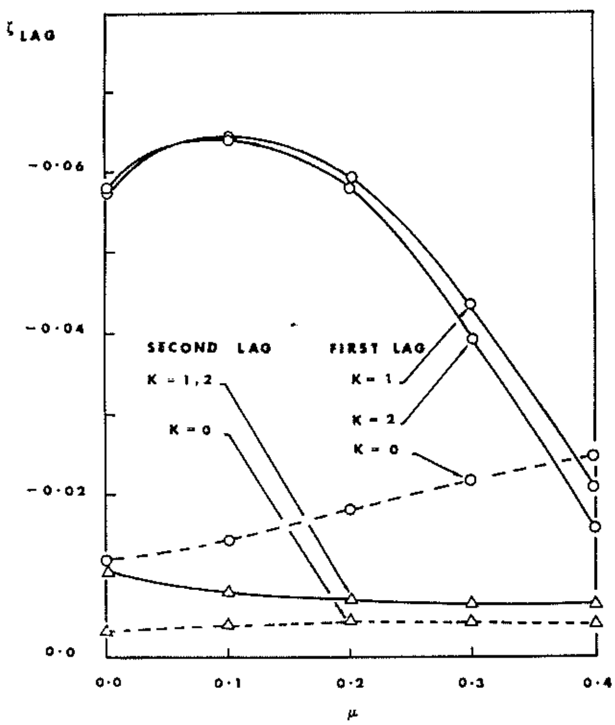

Fig. 21 Blade Stability, Stiff-in-Plane Configuration, Moment Trim, θ_0=8.2°

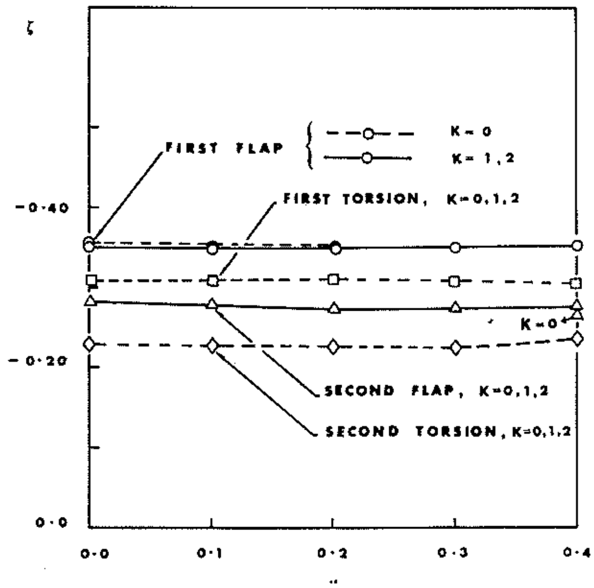

Fig. 20 Blade Stability, Soft-in-Plane Configuration, Moment Trim, θ_0=8.2°

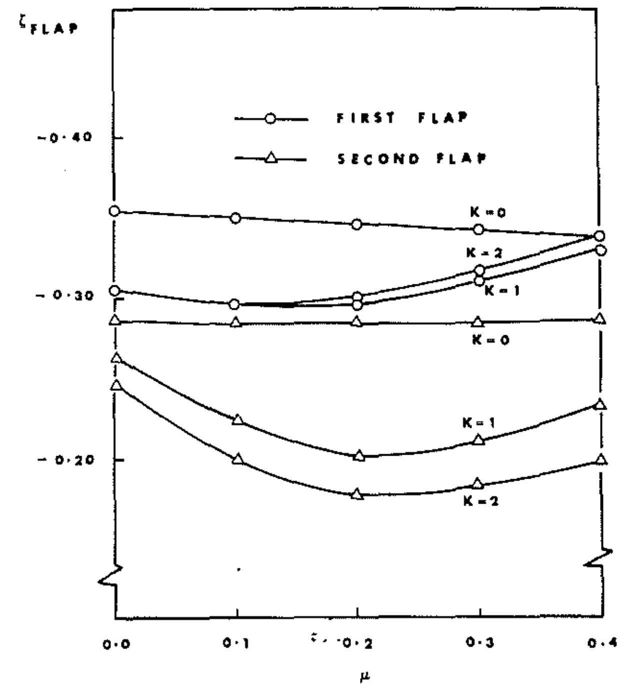

Fig. 22 Blade Stability, Stiff-in-Plane Configuration, Moment Trim, θ_0=8.2°

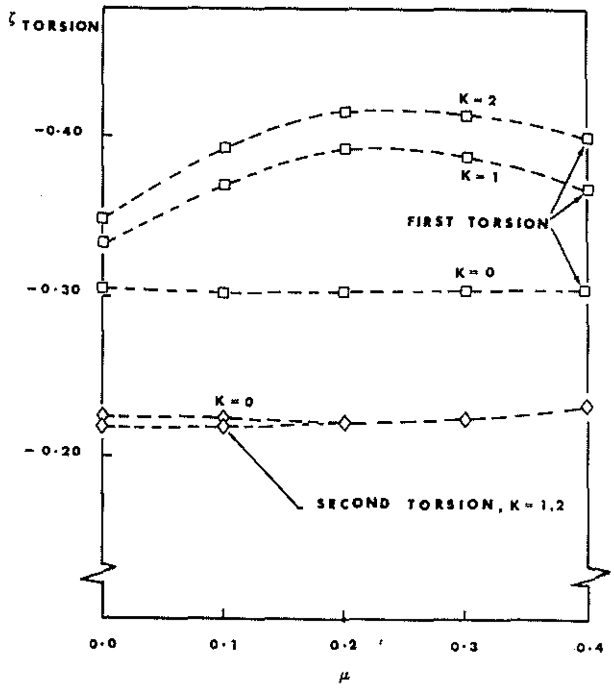

Fig. 23 Blade Stability, Stiff-in-Plane Configuration, Moment Trim, θ_0=8.2°

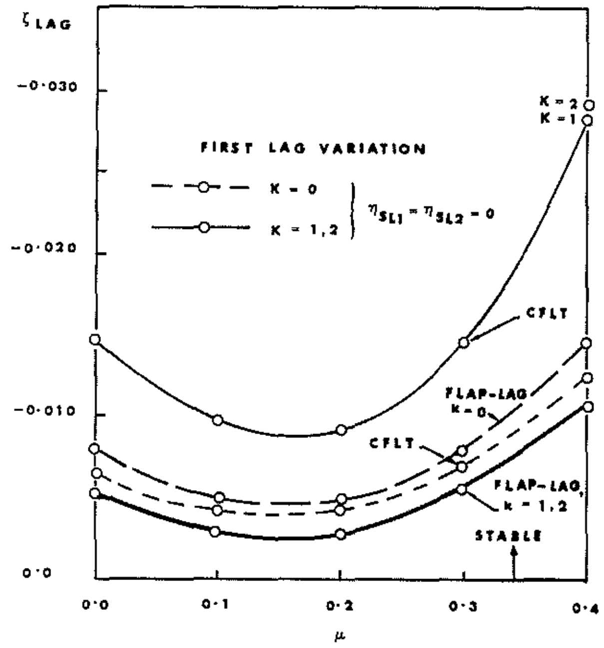

Fig. 24 Blade Stability, Soft-in-Plane Configuration, Comparison of Flap-Lag and Coupled Flap-Lag-Torsion Analyses, Propulsive Trim, C_W=0.005

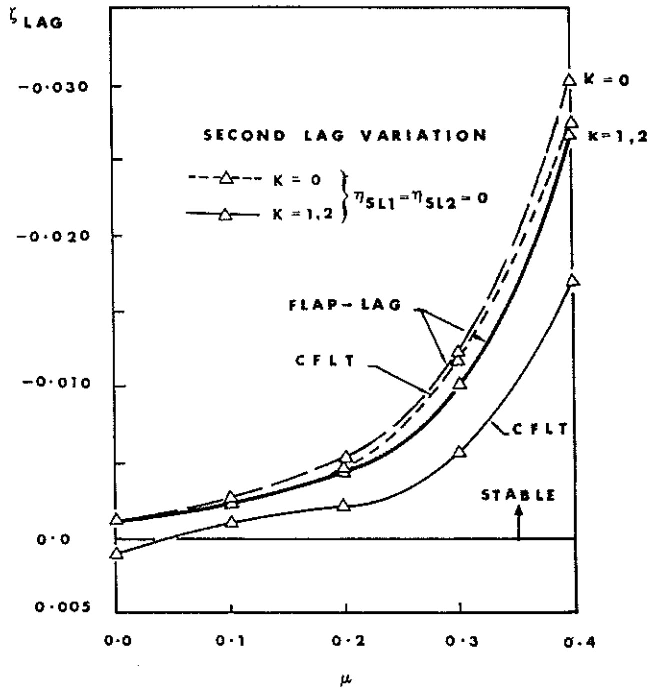

Fig. 25 Blade Stability, Soft-in-Plane Configuration, Comparison of Flap-Lag and Coupled Flap-Lag-Torsion Analyses, Propulsive Trim, C_W=0.005

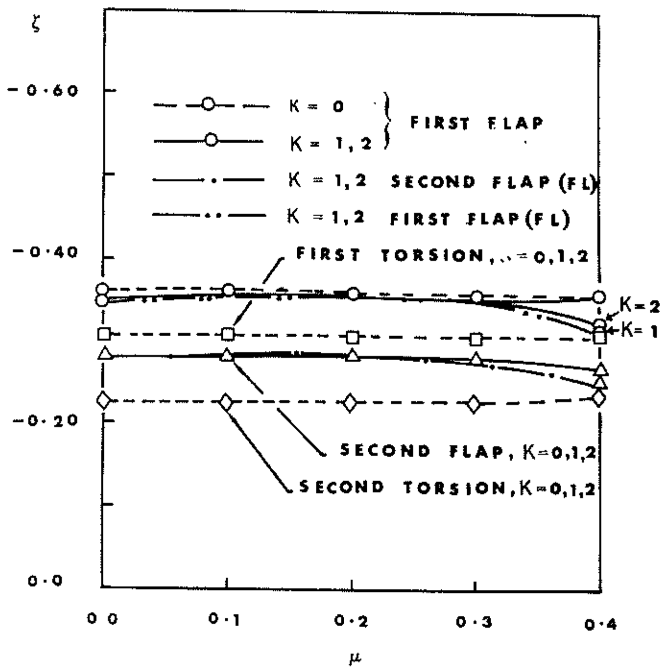

Fig. 26 Blade Stability, Soft-in-Plane Configuration, Comparison of Flap-Lag and Coupled Flap-Lag-Torsion Analyses, Propulsive Trim C_W=0.005